Unitary versus pseudounitary time evolution and statistical effects in the dynamical Sauter-Schwinger process

K. Krajewska and J. Z. Kamiński
Institute of Theoretical Physics, Faculty of Physics, University of Warsaw, Pasteura 5, 02-093 Warszawa, Poland

(Received 26 September 2019; published 13 December 2019)

The dynamical Sauter-Schwinger mechanism of pair creation by a time-dependent electric field composed of N_{rep} identical pulses is analyzed within the framework of spinor and scalar quantum electrodynamics. For linearly polarized pulses, both theories predict that a single eigenmode of the matter wave follows the dynamics of a two-level system. This dynamics, however, is governed by either a Hermitian (for spin-1/2 particles) or a pseudo-Hermitian (for spin-zero particles) Hamiltonian. Essentially, both theories lead to a Fraunhofer-type enhancement of the momentum distributions of created pairs. While in the fermionic case the enhancement is never perfect and it deteriorates with increasing the number of pulses in a train N_{rep}, in the bosonic case we observe the opposite. More specifically, it is at exceptional points where the spectra of bosonic pairs scale exactly as N_{rep}^2, and this scaling is even enhanced with increasing the number of pulses in a train.

DOI: 10.1103/PhysRevA.100.062116

I. INTRODUCTION

Diffraction and interference of waves [1] have played fundamental roles in the development of science. While both phenomena have been observed for sound [2] and surface waves [3], it is the diffraction and interference of light discovered by Grimaldi (1665) and Young (1800) (see [4,5] for details) that paved the way to the development of modern physics. Both phenomena are present, for instance, in light scattering by a diffraction grating. Specifically, in the far-field zone, the resulting intensity of the monochromatic light scattered by N_{rep} parallel slits can be described by the Fraunhofer formula [1]

$$I(u) = I_0 D(u)\left[\frac{\sin(N_{\mathrm{rep}}\pi a u)}{\sin(\pi a u)}\right]^2. \tag{1}$$

Here, $u = \sin\theta/\lambda$ is related to the scattering angle θ and the wavelength of the incident wave λ, a is the distance between two subsequent slits, whereas I_0 is the incident light intensity. The Fraunhofer formula essentially consists of two factors. One of them, $(\frac{\sin(N_{\mathrm{rep}}\pi a u)}{\sin(\pi a u)})^2$, is called the *interference term*. It is responsible for the coherent N_{rep}^2-type enhancement of the scattered wave if detected at the angle θ such that au is an integer. The factor $D(u)$, on the other hand, is called the *diffraction factor*. It describes the wave scattering off a single slit. It depends only on the shape of the individual slit, provided that the neighboring slits are sufficiently well separated from each other. In most cases $D(u)$ is a slowly varying function of u, as opposed to the rapidly changing interference term. For this reason the general pattern (1) consists of well-separated and narrow interference peaks, the intensities of which are modulated by the diffraction term. It appears, however, that in some cases (for instance, when the linear size of the slits becomes comparable to their separation) the diffraction term also exhibits sharp peaks. In such circumstances the distinction between the diffraction and interference peaks is rather difficult to trace. This may lead to misinterpretation of some features of the pattern (1), as we shall discuss in our paper.

With the emergence of quantum theories and the discovery of wave properties of matter, the investigation of diffraction and interference phenomena of matter waves became very important from the fundamental as well as the practical point of view; the point being that these phenomena have prompted some unexpected observations and applications (see, e.g., [6–9]), such as in low-energy [10] or high-energy [11] scattering. Another example is the so-called diffraction radiation [12], which is emitted when charged particles move in vacuum along a periodically deformed surface, the latter playing the role of a diffraction grating. This is known as the Smith-Purcell effect [13] and it can be applied, for instance, for the generation of terahertz radiation, which finds considerable interest in physics, chemistry, and biology [14]. Closely related to the Smith-Purcell effect is the generation of coherent frequency combs of radiation in the scenario in which electrons (or other charged particles) interact with a train of strong laser pulses. In such a case the pulse train acts as a diffraction grating in the time domain [15,16]. Note that the coherent frequency combs of radiation generated from Compton or Thomson scattering offer a possibility for the diagnosis of relativistically intense and short laser pulses [17]. Moreover, similar combs have been observed for matter waves. Specifically, the multislit interference and diffraction pattern, as the one predicted by Eq. (1), has been observed in the momentum and energy distributions of particles emitted via the Breit-Wheeler electron-positron pair creation [18] or in photoionization [19,20]. These selected examples show that the Fraunhofer formula (1) is universal, as it can be applied across different areas of classical and quantum physics.

The aim of this paper is to investigate the quantum vacuum instabilities caused by the action of time-dependent electric

2469-9926/2019/100(6)/062116(15)

fields, the process known as the dynamical Sauter-Schwinger pair creation. Originally considered in a static electric field, it has been a long-standing but still unobserved prediction of strong-field quantum electrodynamics (QED) [21–23]. This follows from the fact that the effect is very weak and in order to observe a sizable number of pairs expelled from vacuum an enormous electric field ($\approx 10^{18}$ V/m) is required. While there are hopes to generate ultrastrong electric fields using next generation lasers, it seems more promising to produce them in heavy-ion collisions [24–27]. In this case, the quark-gluon plasma is formed, which offers a possibility of bosonic pair creation. Another point is that various relativistic predictions can be tested in essentially nonrelativistic systems and configurations. In light of this paper, it is particularly important to mention the electron-hole formation in graphene by external laser fields [28,29]. In this case, the Sauter-Schwinger scenario of pair production can be realized for moderate laser fields, which are typically treated in the dipole approximation, thus neglecting the magnetic component of the laser wave and its space dependence. Taking into account these various perspectives, our focus in this paper is on interference-related enhancements in the dynamical Sauter-Schwinger process.

It has been demonstrated that the multislit interference and diffraction pattern in the momentum distribution of created particles is observed when a finite sequence of electric-field pulses interacts with the vacuum [30–36]. Here, we generalize our recent results [34,35] by comparing theoretical approaches toward particle-antiparticle pair creation based on either spinor or scalar QED. In other words, we are interested in investigating the effect of statistics on the Fraunhofer-type enhancements in pair production. In this context, it is important to mention the paper by Li *et al.* [32], where such effects were already studied. This was done by solving the quantum Vlasov equation [37]. The main conclusion of [32] was that, while the momentum distributions of scalar and spinor particles exhibit very similar Fraunhofer peak patterns, they are shifted relative to each other. Such shifting was ascribed to different statistics of produced particles. However, as we will show, for the parameters considered in our paper this is not necessarily the case. Instead, we shall focus on a fundamental difference between both theories, which is the unitary versus pseudounitary time evolution of the respective fermionic and bosonic fields. Its consequences on the resulting Fraunhofer-like enhancements described above will be studied in this paper in great detail.

Note that our paper fits nicely in the growing area of research devoted to non-Hermitian quantum theories; the reason being that in the case of scalar pair production the dynamics of a single eigenmode of the bosonic field is determined by a pseudo-Hermitian Hamiltonian [Eq. (52)]. Thus, our paper adds to a long list of potential applications of pseudo-Hermitian theories that includes generalized coherent states [38], synthetic optical lattices [39,40], waveguide couplers [41,42], laser cavities [43,44], and Rabi systems [45,46] (for more applications, see also [47–49]). Interestingly, in this context the role of the so-called exceptional points is frequently studied [43,44,50]. While non-Hermitian Hamiltonians have complex eigenvalues, at those points their eigenvalues coalesce. In other words, they exhibit a *nonavoided crossing* where their real components are identical, as are their imaginary ones. This leads to counterintuitive effects when steering the system in the vicinity of the exceptional points (see, for instance, [43,44]). As we show in this paper, the exceptional points are also found in the dynamical pair production of spin-zero particles, and it is only at those points that the fully coherent enhancement of the respective particle spectra is observed. Note that our problem relies on studying a two-state dynamics. Therefore, the conclusions drawn from our results apply essentially to any system such that its dynamics can be traced back to that of a two-level system.

The paper is organized as follows. In Sec. II, we shall present the theoretical formulation of the dynamical Sauter-Schwinger process using scalar and spinor QED. Momentum distributions of created pairs based on both these theories will be presented in Sec. III. Also in Sec. III, we will provide an analytical explanation of our numerical results arising from the analysis of the operators that evolve in time bosonic and fermionic fields. The properties of the bosonic operator will be analyzed in detail in the Appendix whereas for the fermionic case we refer the reader to [34]. In Sec. IV, we will summarize our results.

The numerical results will be expressed in relativistic units. Specifically, we shall use the Sauter-Schwinger electric-field strength $\mathcal{E}_S = m_e^2 c^3/|e|\hbar$, with the corresponding strength of the vector potential, $A_S = m_e c/|e|$, as well as the Compton time $t_C = \hbar/m_e c^2$. Here, m_e is the electron mass and $e = -|e| < 0$ is its charge. From now on, in our theoretical formulation we shall keep $\hbar = 1$ and an arbitrary mass of created particles m. However, we will choose $m = m_e = c = \hbar = 1$ in our numerical calculations.

II. THEORETICAL FORMULATION

The spontaneous formation of particle-antiparticle pairs by a homogeneous in space, time-dependent electric field is studied in this paper within the scalar and the spinor QED frameworks. In order to elucidate the differences between both approaches, we present below both theoretical formulations. Typically, such comparison has been performed within the quantum kinetic approach; thus concealing very subtle but fundamental features of quantum dynamics. Here, we extend our previous studies [34,35] to scalar QED. As we show, while the spinor QED facilitates a typical unitary time evolution of the respective fermionic field eigenmodes [34,35], the respective time evolution of the bosonic field eigenmodes is pseudounitary.

A. Electric-field description

We consider an electric field which oscillates linearly along the z direction, $\boldsymbol{\mathcal{E}}(t) = \mathcal{E}(t)\boldsymbol{e}_z$. In addition, we assume that it satisfies the condition

$$\int_{-\infty}^{+\infty} dt\, \mathcal{E}(t) = 0. \tag{2}$$

If the electric field is defined as

$$\mathcal{E}(t) = \mathcal{E}_0 F(t), \tag{3}$$

where $\mathcal{E}_0$ is the field amplitude whereas $F(t)$ is its shape function, then it follows from (2) that

$$\int_{-\infty}^{+\infty} dt\, F(t) = 0. \tag{4}$$

The significance of Eqs. (2) and (4) becomes clear when we introduce the vector potential; namely, $\boldsymbol{A}(t) = A(t)\boldsymbol{e}_z$ where $\mathcal{E}(t) = -dA(t)/dt$. In other words, if

$$A(t) = \mathcal{E}_0 f(t), \tag{5}$$

then

$$f(t) = f(+\infty) + \int_t^{+\infty} dt' F(t'). \tag{6}$$

Here, taking into account Eq. (4), we conclude that $f(-\infty) = f(+\infty)$. This means that in the remote past and in the far future

$$\lim_{t\to-\infty} A(t) = \lim_{t\to+\infty} A(t). \tag{7}$$

Without losing the generality, we can set this constant to zero and, equivalently, $f(-\infty) = f(+\infty) = 0$. In such case, the behavior of the vector potential $A(t)$ guarantees that our asymptotic "in" and "out" states will be indeed field-free states. This is particularly important for the Sauter-Schwinger pair creation and, hence, it justifies imposing the condition (2).

In the following, we shall consider a single pulse with the shape function in (3) given by

$$F_1(t) = \exp\Big[-\Big(\frac{t - T_0/2}{\sigma}\Big)^{2M}\Big] - \exp\Big[-\Big(\frac{t + T_0/2}{\sigma}\Big)^{2M}\Big]. \tag{8}$$

Note that each half pulse is given by either a Gaussian ($M = 1$) or a super-Gaussian ($M > 1$) envelope, with a duration σ and a time delay between them T_0. An interesting property of super-Gaussian envelopes is that, while they remain smooth functions [of class $C^\infty(\mathbb{R})$], they approach the step function

$$S(t) = \begin{cases} 1, & t \in [-\sigma, \sigma] \\ 0, & t \notin [-\sigma, \sigma] \end{cases} \tag{9}$$

for large M. This is illustrated in the upper panel of Fig. 1. In the lower panel, we present the time dependence of the corresponding vector potential (5). The difference between both columns in Fig. 1 is the time delay T_0 between both half pulses.

Similarly, we shall also consider a train consisting of $N_{\rm rep}$ such pulses, with

$$F_{N_{\rm rep}}(t) = \mathcal{N} \sum_{\ell=1}^{N_{\rm rep}} F_1\Big\{t + \Big[\ell - \frac{1}{2}(N_{\rm rep} + 1)\Big]T\Big\}. \tag{10}$$

Here, the normalization constant $\mathcal{N}$ is chosen such that

$$\max_t |F_{N_{\rm rep}}(t)| = 1, \tag{11}$$

to make sure that the maximum intensity of the electric field is independent of the parameters chosen in the above definitions. In Fig. 2, we represent the respective sequence of two pulses ($N_{\rm rep} = 2$). Again, both columns in the figure are plotted for different values of T_0 (and T). This obviously has to influence the interference-diffraction pattern observed in the momentum distributions of created particles, the details of which will be presented in Sec. III B.

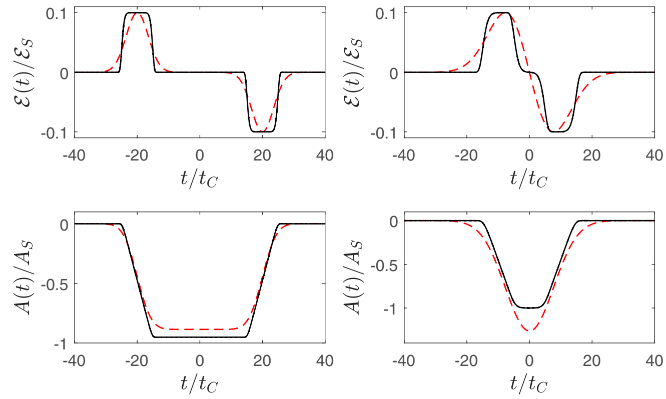

FIG. 1. Time dependence of the electric field $\mathcal{E}(t)$ and the vector potential $A(t)$ (in relativistic units) for a single pulse considered in this paper ($N_{\rm rep} = 1$). The shape functions in (8) are for $\sigma = 5/t_C$, $T_0 = 40t_C$ (left column) and for $\sigma = 10/t_C$, $T_0 = 10t_C$ (right column). In both cases, the amplitude of the electric field is $\mathcal{E}_0 = -0.1\mathcal{E}_S$. Also, the dashed lines are for $M = 1$, whereas the solid lines are for $M = 5$. As one can see, with increasing M, the shape of super-Gaussian envelopes becomes similar to the rectangular one. The qualitative difference between both columns is that, while in the left column both half pulses are well separated in time, in the right column they overlap. In other words, the single pulse in the left column is much longer that the one on the right. As we will show later, this will strongly affect the structure of diffraction patterns observed in the momentum distributions of created pairs.

This model of the oscillating in time electric field will be used in Sec. III B to illustrate the general theory derived in the next two sections. At first, we shall consider the bosonic pair creation. Its rigorous treatment is based on the Klein-Gordon equation, which is the foundation of scalar QED.

B. Scalar QED

We define the Klein-Gordon boson field operator $\hat{\Phi}(x)$ as

$$\hat{\Phi}(x) = \int \frac{d^3\boldsymbol{p}}{(2\pi)^3}[\Phi_{\boldsymbol{p}}^{(+)}(x)\hat{b}_{\boldsymbol{p}} + \Phi_{\boldsymbol{p}}^{(-)}(x)\hat{d}_{-\boldsymbol{p}}^{\dagger}], \tag{12}$$

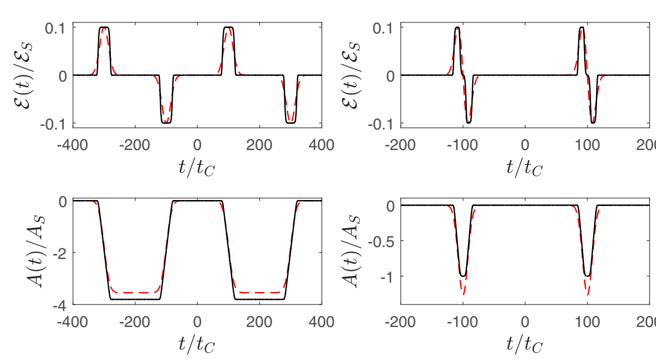

FIG. 2. The same as in Fig. 1 but for a sequence of two pulses [$N_{\rm rep} = 2$ in Eq. (10)]. In addition, we have $\sigma = 20/t_C$, $T_0 = 200t_C$, $T = 400t_C$ (left column) and $\sigma = 10/t_C$, $T_0 = 10t_C$, $T = 200t_C$ (right column). The remaining parameters of the field are the same as in Fig. 1.

where $\Phi_{\boldsymbol{p}}^{(\pm)}(x)$ are the one-particle solutions of the Klein-Gordon equation, whereas $\hat{b}_{\boldsymbol{p}}$ ($\hat{d}_{\boldsymbol{p}}$) is the annihilation operator of a boson (antiboson) with a given momentum $\boldsymbol{p}$. These operators define the in-vacuum state through the conditions $\hat{b}_{\boldsymbol{p}}|0_{-\infty}\rangle = 0$ and $\hat{d}_{\boldsymbol{p}}|0_{-\infty}\rangle = 0$. They also satisfy the commutation relations

$$[\hat{b}_{\boldsymbol{p}}, \hat{b}^{\dagger}_{\boldsymbol{p}'}] = [\hat{d}_{\boldsymbol{p}}, \hat{d}^{\dagger}_{\boldsymbol{p}'}] = \delta^{(3)}(\boldsymbol{p}-\boldsymbol{p}'), \tag{13}$$

with the remaining commutators equal to zero. $\Phi_{\boldsymbol{p}}^{\pm}(x)$, on the other hand, will be constructed in the next section.

1. One-particle solutions of the Klein-Gordon equation

Our aim is to solve the scalar Klein-Gordon equation coupled to the external electromagnetic field:

$$[(i\partial - eA)^2 - (mc)^2]\Phi(x) = 0. \tag{14}$$

Since the problem has translational symmetry, one can look for those solutions $\Phi(x)$ in the separable form

$$\Phi(x) = e^{i\boldsymbol{p}\cdot\boldsymbol{x}}\Phi_{\boldsymbol{p}}(t), \tag{15}$$

where $\boldsymbol{p}$ is the particle asymptotic momentum. Substituting (15) into (14), we obtain that the function $\Phi_{\boldsymbol{p}}(t)$ satisfies the harmonic oscillator equation

$$\left[\frac{d^2}{dt^2} + \omega_{\boldsymbol{p}}^2(t)\right]\Phi_{\boldsymbol{p}}(t) = 0, \tag{16}$$

with the time-dependent frequency $\omega_{\boldsymbol{p}}(t)$:

$$\omega_{\boldsymbol{p}}(t) = \sqrt{(mc^2)^2 + c^2\boldsymbol{p}_{\perp}^2 + c^2[p_{\parallel} - eA(t)]^2}. \tag{17}$$

Here, we have introduced the longitudinal $p_{\parallel}$ and the transverse $\boldsymbol{p}_{\perp}$ components of the particle asymptotic momentum such that

$$p_{\parallel} = \boldsymbol{p}\cdot\boldsymbol{e}_z, \quad \boldsymbol{p}_{\perp} = \boldsymbol{p} - p_{\parallel}\boldsymbol{e}_z. \tag{18}$$

To interpret the solutions of Eq. (16), we realize that in the remote past ($t \to -\infty$) this equation becomes

$$\left[\frac{d^2}{dt^2} + \omega_{\boldsymbol{p}}^2\right]\Phi_{\boldsymbol{p}}(t) = 0, \tag{19}$$

where

$$\omega_{\boldsymbol{p}} = \sqrt{(mc^2)^2 + c^2\boldsymbol{p}^2}. \tag{20}$$

Therefore, there exist two linearly independent solutions of Eq. (19) which we will label by the parameter β:

$$\Phi_{\boldsymbol{p}}^{(\beta)}(t) \underset{t\to-\infty}{\sim} e^{-i\beta\omega_{\boldsymbol{p}}t}. \tag{21}$$

The one corresponding to a positive energy (with β=+) will be interpreted as a boson whereas the other one (with β=−) will be interpreted as an antiboson. In this way, we have determined two sets of solutions of the Klein-Gordon equation that appear in (12):

$$\Phi_{\boldsymbol{p}}^{(\beta)}(x) = e^{i\boldsymbol{p}\cdot\boldsymbol{x}}\Phi_{\boldsymbol{p}}^{(\beta)}(t), \tag{22}$$

where $\Phi_{\boldsymbol{p}}^{(\beta)}(t)$ solves Eq. (16) and asymptotically behaves according to (21). Note that we have chosen the same symbol for the space-time- and time-dependent solutions, discriminating them by the argument $x = (ct, \boldsymbol{x})$ and t.

It is crucial that $\Phi_{\boldsymbol{p}}^{(\beta)}(x)$ form an orthonormal and complete set of solutions of the Klein-Gordon equation. This is provided that the inner product of two such wave functions, $\Phi_{\boldsymbol{p}}^{(\beta)}(x)$ and $\Phi_{\boldsymbol{p}'}^{(\beta')}(x)$, is defined as [51–54]

$$\begin{aligned}\langle\Phi_{\boldsymbol{p}}^{(\beta)}|\Phi_{\boldsymbol{p}'}^{(\beta')}\rangle &= i\int d^3\boldsymbol{x}\,[\Phi_{\boldsymbol{p}}^{(\beta)}(x)]^*\overleftrightarrow{\partial_0}\,\Phi_{\boldsymbol{p}'}^{(\beta')}(x)\\ &= i\int d^3\boldsymbol{x}\,\{[\Phi_{\boldsymbol{p}}^{(\beta)}(x)]^*[\partial_0\Phi_{\boldsymbol{p}'}^{(\beta')}(x)]\\ &\quad - [\partial_0\Phi_{\boldsymbol{p}}^{(\beta)}(x)]^*\Phi_{\boldsymbol{p}'}^{(\beta')}(x)\}.\end{aligned} \tag{23}$$

Its physical significance can be realized when considering the four-current density of charge, $j^{\mu}(x)$. In the absence of the external electromagnetic field, it is defined as [53,54]

$$j^{\mu}(x) = \frac{ie}{2m}\{\Phi_{\boldsymbol{p}}^{(\beta)*}(x)[\partial^{\mu}\Phi_{\boldsymbol{p}}^{(\beta)}(x)] - [\partial^{\mu}\Phi_{\boldsymbol{p}}^{(\beta)*}(x)]\Phi_{\boldsymbol{p}}^{(\beta)}(x)\}, \tag{24}$$

where $j^{\mu}(x)$ satisfies the continuity equation

$$\partial_{\mu}j^{\mu}(x) = 0. \tag{25}$$

Taking into account (22), it follows from this equation that the quantity

$$Q = \int d^3\boldsymbol{x}\,j^0(x) \tag{26}$$

is conserved. Since $j^0(x)$ can take either positive or negative values, it cannot be identified with the probability density. Instead, if we reinterpret the Klein-Gordon equation as satisfied by a quantum field $\hat{\Phi}(x)$, $\hat{j}^0(x)$ will describe the charge density of the field, whereas $\hat{Q}$ will be the field charge [53,54]. Going back to the definition of the Klein-Gordon inner product (23), we see therefore that it is related to the conservation of the field charge Q. In the presence of the electromagnetic field, the four-vector current density has to be redefined:

$$\begin{aligned}j^{\mu}(x) = \frac{ie}{2m}\{\Phi_{\boldsymbol{p}}^{(\beta)*}(x)[\partial^{\mu}\Phi_{\boldsymbol{p}}^{(\beta)}(x)] - [\partial^{\mu}\Phi_{\boldsymbol{p}}^{(\beta)*}(x)]\Phi_{\boldsymbol{p}}^{(\beta)}(x)\}\\ - \frac{e^2}{mc}A^{\mu}(x)|\Phi_{\boldsymbol{p}}^{(\beta)}(x)|^2.\end{aligned} \tag{27}$$

Nevertheless, for as long as $A^0(x) = 0$, which is the case discussed here, the definition of the Klein-Gordon inner product (23) does not change.

Keeping this in mind, we obtain for the inner product of the scalar wave functions (23)

$$\begin{aligned}\langle\Phi_{\boldsymbol{p}}^{(\beta)}|\Phi_{\boldsymbol{p}'}^{(\beta')}\rangle = (2\pi)^3\delta^{(3)}(\boldsymbol{p}-\boldsymbol{p}')\bigg\{\frac{i}{c}[\Phi_{\boldsymbol{p}}^{(\beta)}(t)]^*\dot{\Phi}_{\boldsymbol{p}}^{(\beta')}(t)\\ - \frac{i}{c}[\dot{\Phi}_{\boldsymbol{p}}^{(\beta)}(t)]^*\Phi_{\boldsymbol{p}}^{(\beta')}(t)\bigg\}.\end{aligned} \tag{28}$$

Using Eqs. (16) and (28), one can show that

$$\frac{d}{dt}\left\{\frac{i}{c}[\Phi_{\boldsymbol{p}}^{(\beta)}(t)]^*\dot{\Phi}_{\boldsymbol{p}}^{(\beta')}(t) - \frac{i}{c}[\dot{\Phi}_{\boldsymbol{p}}^{(\beta)}(t)]^*\Phi_{\boldsymbol{p}}^{(\beta')}(t)\right\} = 0, \tag{29}$$

where the dot stands for time derivative. It follows from this equation that the quantity in the brackets is constant in time. Setting its value at $t \to -\infty$ gives

$$\lim_{t\to-\infty}\left\{\frac{i}{c}\big[\Phi_{\boldsymbol p}^{(\beta)}(t)\big]^*\dot\Phi_{\boldsymbol p}^{(\beta')}(t)-\frac{i}{c}\big[\dot\Phi_{\boldsymbol p}^{(\beta)}(t)\big]^*\Phi_{\boldsymbol p}^{(\beta')}(t)\right\} = \frac{2\omega_{\boldsymbol p}}{c}\beta\delta_{\beta\beta'}. \tag{30}$$

Hence, the one-particle solutions of the Klein-Gordon equation $\Phi_{\boldsymbol p}^{(\beta)}(x)$ can be normalized such that

$$i\int d^3\boldsymbol x\,\big[\Phi_{\boldsymbol p}^{(\beta)}(x)\big]^*\overleftrightarrow{\partial_0}\,\Phi_{\boldsymbol p'}^{(\beta')}(x)=2mc\beta(2\pi)^3\delta^{(3)}(\boldsymbol p-\boldsymbol p')\delta_{\beta\beta'}. \tag{31}$$

Finally, we write down the completeness relation for these wave functions:

$$\frac{1}{2mc}\sum_\beta\int\frac{d^3\boldsymbol p}{(2\pi)^3}\,i\beta\Phi_{\boldsymbol p}^{(\beta)}(x)\overleftrightarrow{\partial_0}\big[\Phi_{\boldsymbol p'}^{(\beta')}(x)\big]^*=\delta^{(3)}(\boldsymbol x-\boldsymbol x'). \tag{32}$$

Since the one-particle solutions of the Klein-Gordon equation (22) form a complete and orthonormal set of functions (see also [51,52]), one can use them to construct the boson field operator (12).

2. Bogoliubov transformation for the boson field

The instantaneous Hamiltonian of the bosonic field in the presence of an external time-dependent electric field is given by [53]

$$\hat H(t)=\frac{1}{2m}\int d^3\boldsymbol x\left(\frac{1}{c^2}\dot{\hat\Phi}^\dagger(x)\dot{\hat\Phi}(x)+\hat\Phi^\dagger(x)\{[\hat{\boldsymbol p}-e\boldsymbol A(t)]^2+(mc)^2\}\hat\Phi(x)\right). \tag{33}$$

Substituting here (12), we arrive at

$$\hat H(t)=\int\frac{d^3\boldsymbol p}{(2\pi)^3}\big[\gamma_{\boldsymbol p}^{(++)}(t)\hat b_{\boldsymbol p}^\dagger\hat b_{\boldsymbol p}+\gamma_{\boldsymbol p}^{(+-)}(t)\hat b_{\boldsymbol p}^\dagger\hat d_{-\boldsymbol p}^\dagger+\gamma_{\boldsymbol p}^{(-+)}(t)\hat d_{-\boldsymbol p}\hat b_{\boldsymbol p}+\gamma_{\boldsymbol p}^{(--)}(t)\hat d_{-\boldsymbol p}\hat d_{-\boldsymbol p}^\dagger\big], \tag{34}$$

where the time-dependent coefficients $\gamma_{\boldsymbol p}^{(\beta\beta')}(t)$ are defined as

$$\gamma_{\boldsymbol p}^{(\beta\beta')}(t)=\begin{cases}\dfrac{1}{2mc^2}\big[\big|\dot\Phi_{\boldsymbol p}^{(\beta)}(t)\big|^2+\omega_{\boldsymbol p}^2(t)\big|\Phi_{\boldsymbol p}^{(\beta)}(t)\big|^2\big] & \text{if } \beta=\beta'\\[2mm] \dfrac{1}{2mc^2}\{\big[\dot\Phi_{\boldsymbol p}^{(\beta)}(t)\big]^*\dot\Phi_{\boldsymbol p}^{(\beta')}(t)+\omega_{\boldsymbol p}^2(t)\big[\Phi_{\boldsymbol p}^{(\beta)}(t)\big]^*\Phi_{\boldsymbol p}^{(\beta')}(t)\} & \text{if } \beta\neq\beta'\end{cases}. \tag{35}$$

One can show using the asymptotic condition (21) that

$$\lim_{t\to-\infty}\gamma_{\boldsymbol p}^{(\beta\beta')}(t)=\omega_{\boldsymbol p}\delta_{\beta\beta'}, \tag{36}$$

where we have used the normalization of the asymptotic solution in compliance with (47) in order to eliminate $1/mc^2$. Thus, in the remote past the Hamiltonian (34) describes a free bosonic field. It is the interaction with the pulsed electric field which leads to the appearance of nondiagonal terms, $\hat b_{\boldsymbol p}^\dagger\hat d_{-\boldsymbol p}^\dagger$ and $\hat d_{-\boldsymbol p}\hat b_{\boldsymbol p}$, in (34). These terms, however, can be removed by means of the Bogoliubov transformation [55].

In order to diagonalize the Hamiltonian (34), we introduce new annihilation operators [55]

$$\hat b_{\boldsymbol p}(t)=\eta_{\boldsymbol p}(t)\hat b_{\boldsymbol p}+\xi_{\boldsymbol p}(t)\hat d_{-\boldsymbol p}^\dagger, \tag{37}$$

$$\hat d_{\boldsymbol p}(t)=\eta_{-\boldsymbol p}(t)\hat d_{\boldsymbol p}+\xi_{-\boldsymbol p}(t)\hat b_{-\boldsymbol p}^\dagger \tag{38}$$

and the corresponding creation operators as well. They are defined through unknown time-dependent functions $\eta_{\boldsymbol p}(t)$ and $\xi_{\boldsymbol p}(t)$. As the instantaneous operators, $\hat b_{\boldsymbol p}(t)$ and $\hat d_{\boldsymbol p}(t)$, should evolve from the corresponding in operators, $\hat b_{\boldsymbol p}$ and $\hat d_{\boldsymbol p}$, we infer that

$$\lim_{t\to-\infty}\eta_{\boldsymbol p}(t)=1,\quad \lim_{t\to-\infty}\xi_{\boldsymbol p}(t)=0. \tag{39}$$

In addition, after imposing the bosonic commutation relations on the new set of annihilation and creation operators, we obtain that at all times

$$|\eta_{\boldsymbol p}(t)|^2-|\xi_{\boldsymbol p}(t)|^2=1. \tag{40}$$

Keeping this in mind, we rewrite the bosonic field operator (12) as

$$\hat\Phi(x)=\int\frac{d^3\boldsymbol p}{(2\pi)^3}\big[\phi_{\boldsymbol p}^{(+)}(x)\hat b_{\boldsymbol p}(t)+\phi_{\boldsymbol p}^{(-)}(x)\hat d_{-\boldsymbol p}^\dagger(t)\big], \tag{41}$$

where the new functions

$$\phi_{\boldsymbol p}^{(+)}(x)=\eta_{\boldsymbol p}^*(t)\Phi_{\boldsymbol p}^{(+)}(x)-\xi_{\boldsymbol p}^*(t)\Phi_{\boldsymbol p}^{(-)}(x), \tag{42}$$

$$\phi_{\boldsymbol p}^{(-)}(x)=\eta_{\boldsymbol p}(t)\Phi_{\boldsymbol p}^{(-)}(x)-\xi_{\boldsymbol p}(t)\Phi_{\boldsymbol p}^{(+)}(x) \tag{43}$$

have been introduced in compliance with the Bogoliubov transformation [Eqs. (37) and (38)]. Moreover, we assume that

$$\phi_{\boldsymbol p}^{(\beta)}(x)=e^{i\boldsymbol p\cdot\boldsymbol x-i\beta\int^t dt'\omega_{\boldsymbol p}(t')}\tilde\phi_{\boldsymbol p}^{(\beta)}(t). \tag{44}$$

Thus, it follows from Eqs. (15), (42), (43), and (44) that

$$\Phi_{\boldsymbol p}^{(+)}(t)=\eta_{\boldsymbol p}(t)e^{-i\int^t dt'\omega_{\boldsymbol p}(t')}\tilde\phi_{\boldsymbol p}^{(+)}(t)+\xi_{\boldsymbol p}^*(t)e^{i\int^t dt'\omega_{\boldsymbol p}(t')}\tilde\phi_{\boldsymbol p}^{(-)}(t), \tag{45}$$

$$\Phi_{\boldsymbol p}^{(-)}(t)=\eta_{\boldsymbol p}^*(t)e^{i\int^t dt'\omega_{\boldsymbol p}(t')}\tilde\phi_{\boldsymbol p}^{(-)}(t)+\xi_{\boldsymbol p}(t)e^{-i\int^t dt'\omega_{\boldsymbol p}(t')}\tilde\phi_{\boldsymbol p}^{(+)}(t). \tag{46}$$

One can show that these functions solve Eq. (16) provided that

$$\tilde\phi_{\boldsymbol p}^{(\beta)}(t)=\sqrt{\frac{mc^2}{\omega_{\boldsymbol p}(t)}}, \tag{47}$$

with the coefficients $\eta_{\boldsymbol{p}}(t)$ and $\xi_{\boldsymbol{p}}(t)$ coupled through the equations

$$\dot{\eta}_{\boldsymbol{p}}(t)=\frac{\dot{\omega}_{\boldsymbol{p}}(t)}{2\omega_{\boldsymbol{p}}(t)}\,\xi^*_{\boldsymbol{p}}(t)e^{2i\int^t dt'\omega_{\boldsymbol{p}}(t')}, \tag{48}$$

$$\dot{\xi}^*_{\boldsymbol{p}}(t)=\frac{\dot{\omega}_{\boldsymbol{p}}(t)}{2\omega_{\boldsymbol{p}}(t)}\,\eta_{\boldsymbol{p}}(t)e^{-2i\int^t dt'\omega_{\boldsymbol{p}}(t')}. \tag{49}$$

This system of equations has to be solved with the initial conditions such that at time t_0, which is before the pulsed electric field starts to act, $\eta_{\boldsymbol{p}}(t_0)=1$ and $\xi_{\boldsymbol{p}}(t_0)=0$. It is useful to introduce new coefficients,

$$c^{(1)}_{\boldsymbol{p}}(t)=\eta_{\boldsymbol{p}}(t)e^{-i\int^t dt'\omega_{\boldsymbol{p}}(t')}, \tag{50}$$

$$c^{(2)}_{\boldsymbol{p}}(t)=\xi^*_{\boldsymbol{p}}(t)e^{i\int^t dt'\omega_{\boldsymbol{p}}(t')}, \tag{51}$$

as it allows us to remove the rapidly oscillating in time phase factors in (48) and (49). In this case, Eqs. (48) and (49) become

$$i\frac{d}{dt}\begin{bmatrix}c^{(1)}_{\boldsymbol{p}}(t)\\ c^{(2)}_{\boldsymbol{p}}(t)\end{bmatrix}=\begin{pmatrix}\omega_{\boldsymbol{p}}(t) & -i\Omega_{\boldsymbol{p}}(t)\\ -i\Omega_{\boldsymbol{p}}(t) & -\omega_{\boldsymbol{p}}(t)\end{pmatrix}\begin{bmatrix}c^{(1)}_{\boldsymbol{p}}(t)\\ c^{(2)}_{\boldsymbol{p}}(t)\end{bmatrix}, \tag{52}$$

where

$$\Omega_{\boldsymbol{p}}(t)=-\frac{\dot{\omega}_{\boldsymbol{p}}(t)}{2\omega_{\boldsymbol{p}}(t)}=-ce\mathcal{E}(t)\frac{c[p_\parallel-eA(t)]}{2\omega^2_{\boldsymbol{p}}(t)}, \tag{53}$$

and we impose the initial conditions such that $c^{(1)}_{\boldsymbol{p}}(t_0)=1$ and $c^{(2)}_{\boldsymbol{p}}(t_0)=0$. At this point it is important to stress that the matrix in Eq. (52) is non-Hermitian, which means the lack of unitarity of the quantum field theory for spin-zero particles. This actually has deep roots, as preservation of the boson commutation relations in the time-dependent base necessitates the nonunitary character of the field time evolution. For more details, we refer the reader to Sec. III and the Appendix.

In closing this section, let us rewrite the instantaneous Hamiltonian (33) using the time-dependent operators. Namely,

$$\hat{H}(t)=\int\frac{d^3\boldsymbol{p}}{(2\pi)^3}\,\omega_{\boldsymbol{p}}(t)[\hat{b}^\dagger_{\boldsymbol{p}}(t)\hat{b}_{\boldsymbol{p}}(t)+\hat{d}^\dagger_{-\boldsymbol{p}}(t)\hat{d}_{-\boldsymbol{p}}(t)], \tag{54}$$

where we have removed an infinite constant by normal ordering the operators $\hat{d}_{-\boldsymbol{p}}(t)$ and $\hat{d}^\dagger_{-\boldsymbol{p}}(t)$. As one can see, at each time t, Eq. (54) represents a collection of harmonic oscillators with energy $\omega_{\boldsymbol{p}}(t)$. Interestingly, the functions which define the Bogoliubov transformation and, thus, allow us to diagonalize the Hamiltonian are obtained from solutions of (52). Hence, for a single eigenmode of the bosonic field, the problem is equivalent to solving a two-level system (52) the dynamics of which is not determined by a unitary matrix. The latter is an element of the SU(1, 1) group, the properties of which are analyzed in the Appendix. Further, we will investigate physical consequences of a nonunitary character of time evolution of the bosonic field as compared to the fermionic case.

3. Normalized charge distribution of created boson pairs

Before we define the quantity that will be analyzed in Sec. III B, we go back to Eqs. (37) and (38). These equations define an instantaneous vacuum state $|0_t\rangle$ such that $\hat{b}_{\boldsymbol{p}}(t)|0_t\rangle=0$ and $\hat{d}_{\boldsymbol{p}}(t)|0_t\rangle=0$. It is different than the in-vacuum state, as

$$\begin{aligned}\hat{b}_{\boldsymbol{p}}(t)|0_{-\infty}\rangle&=\xi_{\boldsymbol{p}}(t)\hat{d}^\dagger_{-\boldsymbol{p}}|0_{-\infty}\rangle,\\ \hat{d}_{\boldsymbol{p}}(t)|0_{-\infty}\rangle&=\xi_{-\boldsymbol{p}}(t)\hat{b}^\dagger_{-\boldsymbol{p}}|0_{-\infty}\rangle.\end{aligned} \tag{55}$$

In addition, the charge field operator can be derived from (26):

$$\hat{Q}=e\int\frac{d^3\boldsymbol{p}}{(2\pi)^3}[\hat{b}^\dagger_{\boldsymbol{p}}(t)\hat{b}_{\boldsymbol{p}}(t)-\hat{d}^\dagger_{-\boldsymbol{p}}(t)\hat{d}_{-\boldsymbol{p}}(t)], \tag{56}$$

where the normal ordering of the creation and annihilation operators has been introduced. As it follows from (55), the mean value of $\hat{Q}$ in the in-vacuum state is zero. One can also show that the charge field operator is conserved during the time evolution. Building upon the definition of (56), we can interpret

$$\begin{aligned}Q^{(0)}(\boldsymbol{p},t)&=e\langle 0_{-\infty}|\hat{b}^\dagger_{\boldsymbol{p}}(t)\hat{b}_{\boldsymbol{p}}(t)|0_{-\infty}\rangle\\ &=e\langle 0_{-\infty}|\hat{d}^\dagger_{-\boldsymbol{p}}(t)\hat{d}_{-\boldsymbol{p}}(t)|0_{-\infty}\rangle\\ &=e|\xi_{\boldsymbol{p}}(t)|^2\delta^{(3)}(\boldsymbol{p})=e\big|c^{(2)}_{\boldsymbol{p}}(t)\big|^2\delta^{(3)}(\boldsymbol{p})\end{aligned} \tag{57}$$

as the charge distribution of created bosons with momentum $\boldsymbol{p}$ and antibosons with momentum $-\boldsymbol{p}$ from the initial vacuum state by the pulsed electric field. Here, we have used Eq. (51). While this accounts for quasiparticles, the charge distribution of a real boson pair is obtained from (57) by taking the limit $t\to+\infty$. Moreover, when considered as a function of $\boldsymbol{p}$, it will be related to the momentum distribution of created bosons. Note the appearance of $\delta^{(3)}(\boldsymbol{p})$. This is related to an infinite volume, in which the pair creation is considered. For the momentum distributions to be finite, we will define them per unit volume. We will refer to it in Sec. III.

C. Spinor QED

The spinor QED formulation of the pair production from vacuum by a time-dependent pulsed electric field has been presented in [34] (see also [51,52]). It is based on the Dirac equation that describes spin-1/2 particles, when coupled to an external electromagnetic field. As it was shown there, the dynamics of a single eigenmode of a fermionic field, specified by the momentum $\boldsymbol{p}$ and the spin projection λ, is defined by two differential equations,

$$i\frac{d}{dt}\begin{bmatrix}c^{(1)}_{\boldsymbol{p}}(t)\\ c^{(2)}_{\boldsymbol{p}}(t)\end{bmatrix}=\begin{pmatrix}\omega_{\boldsymbol{p}}(t) & i\Omega_{\boldsymbol{p}}(t)\\ -i\Omega_{\boldsymbol{p}}(t) & -\omega_{\boldsymbol{p}}(t)\end{pmatrix}\begin{bmatrix}c^{(1)}_{\boldsymbol{p}}(t)\\ c^{(2)}_{\boldsymbol{p}}(t)\end{bmatrix}, \tag{58}$$

that are analogous to Eq. (52). This similarity is due to the fact that, for a linearly polarized electric field, the bispinor part of the fermionic wave function decouples [34,51,52]. Hence, each eigenmode exhibits the same time evolution irrespective of the particle spins λ. This does not hold for a circularly or an elliptically polarized field. In these cases, the Dirac-Heisenberg-Wigner approach [56] and its development based on the spinoral decomposition [57] can be used instead. Going back to Eq. (58), it has to be solved with the same initial conditions as in Sec. II B, $c^{(1)}_{\boldsymbol{p}}(t_0)=1$ and $c^{(2)}_{\boldsymbol{p}}(t_0)=0$. This time, however,

$$\Omega_{\boldsymbol{p}}(t)=-\frac{ce\mathcal{E}(t)\epsilon_\perp}{2\omega^2_{\boldsymbol{p}}(t)}, \tag{59}$$

where $\epsilon_\perp = \sqrt{(c\boldsymbol{p}_\perp)^2 + (mc^2)^2}$. Another difference is that while the matrix governing the time evolution here is Hermitian for the bosonic case it is pseudo-Hermitian [see Eq. (52)]. This, in principle, may have far-reaching consequences which will be studied in detail next.

In closing this section, we note that the charge distribution of created fermion pairs with momenta $\boldsymbol{p}$ and $-\boldsymbol{p}$ for a particle and an antiparticle, respectively, is

$$Q^{(1/2)}(\boldsymbol{p}, t) = e\left|c_{\boldsymbol{p}}^{(2)}(t)\right|^2 \delta^{(3)}(\boldsymbol{p}), \tag{60}$$

where the coefficient $c_{\boldsymbol{p}}^{(2)}(t)$ satisfies (58).

III. MOMENTUM DISTRIBUTIONS OF CREATED PARTICLES

In this section, we shall analyze statistical effects in the electron-positron pair creation from vacuum under the influence of time-dependent, linearly polarized electric-field pulses. For this purpose, we will use the formulations introduced in Secs. II B and II C, treating the pairs as scalar or spinor particles.

Note that the formulas (57) and (60) have been obtained for an infinite volume of quantization. For a finite volume V one has to apply the standard relation $(2\pi)^3\delta^{(3)}(\boldsymbol{p}) = V$. Having this in mind, we define the charge distribution per unit volume:

$$\frac{1}{V} Q^{(s)}(\boldsymbol{p}, t) = \frac{1}{(2\pi)^3} e\left|c_{\boldsymbol{p}}^{(2)}(t)\right|^2, \tag{61}$$

where $Q^{(s)}(\boldsymbol{p}, t)$ is defined by Eq. (57) or (60). Hence, the momentum distribution $\mathcal{P}_{N_{\rm rep}}^{(s)}(\boldsymbol{p})$ and the total number n of particles created per unit volume by a sequence of $N_{\rm rep}$ identical electric pulses are given, respectively, as [51]

$$\mathcal{P}_{N_{\rm rep}}^{(s)}(\boldsymbol{p}) = \lim_{t\to\infty} \left|c_{\boldsymbol{p}}^{(2)}(t)\right|^2 \tag{62}$$

and

$$n = \int \frac{d^3p}{(2\pi)^3} \mathcal{P}_{N_{\rm rep}}^{(s)}(\boldsymbol{p}). \tag{63}$$

Depending on the statistics, which is reflected in a different set of equations being solved for $c_{\boldsymbol{p}}^{(2)}(t)$ [Eq. (52) for spinless particles ($s = 0$) and Eq. (58) for spinor particles ($s = 1/2$)], we may observe different patterns in the momentum distributions (62). For instance, it was shown in [32] that the longitudinal spectra of created bosons and fermions are shifted by $\pi/2$. In relation to those results, we will focus here on the longitudinal spectra as well, i.e., we set $\boldsymbol{p}_\perp = \boldsymbol{0}$. However, before presenting our numerical results we shall derive the Fraunhofer-type formulas for pair creation from vacuum that arise in the scalar and spinor QED.

A. Fraunhofer-type formulas for the scalar and spinor QED

Consider the time-evolution matrix $\hat{U}(t, t_0)$ for a single eigenmode of either the bosonic or fermionic field. In accordance with Eqs. (52) and (58), it satisfies the equation

$$i\frac{d}{dt}\hat{U}(t, t_0) = \begin{pmatrix} \omega_{\boldsymbol{p}}(t) & \mp i\Omega_{\boldsymbol{p}}(t) \\ -i\Omega_{\boldsymbol{p}}(t) & -\omega_{\boldsymbol{p}}(t) \end{pmatrix} \hat{U}(t, t_0), \tag{64}$$

where the upper sign relates to the boson and the lower one relates to the fermion statistics. Note that $\Omega_{\boldsymbol{p}}(t)$ differs in both cases too [Eqs. (53) and (59)]. It follows from (64) that for fermions the time evolution is unitary, meaning that $\hat{U}$ belongs to the SU(2) group (see [34]). However, for bosons this is not the case. One can prove using Eq. (64) that for bosons

$$\frac{d}{dt}[\hat{U}^\ddagger(t, t_0)\hat{U}(t, t_0)] = 0, \tag{65}$$

where the pseudo-Hermitian conjugate of $\hat{U}(t, t_0)$ has been introduced:

$$\hat{U}^\ddagger(t, t_0) = \hat{\sigma}_3 \hat{U}^\dagger(t, t_0)\hat{\sigma}_3, \tag{66}$$

with $\hat{\sigma}_3 = \left(\begin{smallmatrix} 1 & 0 \\ 0 & -1 \end{smallmatrix}\right)$. Hence, accounting for the initial condition $\hat{U}(t_0, t_0) = \hat{I}$, we obtain

$$\hat{U}^\ddagger(t, t_0)\hat{U}(t, t_0) = \hat{I}. \tag{67}$$

This means that $\hat{U}$ is the element of the SU(1, 1) group, discussed in the Appendix. Keeping this in mind, we shall derive now physical consequences of unitary versus pseudounitary time evolution of particles created from the vacuum by a sequence of electric-field pulses.

1. Monodromy matrix

For a train of $N_{\rm rep}$ identical electric-field pulses, each of time duration T, both functions $\Omega_{\boldsymbol{p}}(t)$ and $\omega_{\boldsymbol{p}}(t)$ in (64) are periodic within the time interval $N_{\rm rep}T$, with a period T. Hence, the same applies to $\hat{U}(t, t_0)$. This property combined with the composition condition for the time-evolution operators results in

$$\begin{aligned} \hat{U}(N_{\rm rep}T + t_0, t_0) &= \prod_{j=0}^{N_{\rm rep}-1} \hat{U}((j+1)T + t_0, jT + t_0) \\ &= [\hat{U}(T + t_0, t_0)]^{N_{\rm rep}}, \end{aligned} \tag{68}$$

where we shall refer to $\hat{U}(T + t_0, t_0)$ as the *monodromy matrix* [58]. This matrix is evaluated at the period of the interaction with the external electric field. As a consequence of (68), it determines the system evolution under the influence of a finite sequence of well-separated electric-field pulses.

The monodromy matrix in the fermionic case has been introduced in [34]. It was shown there that it can be parametrized using four real parameters such that $0 \leqslant \vartheta_0, \vartheta, \beta < 2\pi$ and $0 \leqslant \gamma \leqslant \pi$:

$$\hat{U}(T + t_0, t_0) = e^{-i\vartheta_0} \begin{pmatrix} \cos\vartheta + i\sin\vartheta\cos\gamma & ie^{-i\beta}\sin\vartheta\sin\gamma \\ ie^{i\beta}\sin\vartheta\sin\gamma & \cos\vartheta - i\sin\vartheta\cos\gamma \end{pmatrix}. \tag{69}$$

One can check that its eigenvalues are

$$\begin{aligned}\lambda_1 &= e^{-i\vartheta_1} \quad \text{with} \quad \vartheta_1 = \vartheta_0 - \vartheta,\\ \lambda_2 &= e^{-i\vartheta_2} \quad \text{with} \quad \vartheta_2 = \vartheta_0 + \vartheta,\end{aligned} \tag{70}$$

meaning that $|\lambda_{1,2}| = 1$. As it was presented in [34], the respective phases $\vartheta_1, \vartheta_2 \in \mathbb{R}$ play a significant role in interpreting interference patterns in the momentum distributions of created fermions. The same is true for bosons. The difference, however, is that for bosons the phases ϑ_1 and ϑ_2 are not necessarily real.

As shown in the Appendix, the pseudounitary monodromy matrix for bosons can be parametrized either as

$$\hat{U}(T+t_0,t_0) = e^{-i\vartheta_0}\begin{pmatrix} \cos\vartheta + i\sin\vartheta\cosh\gamma & -ie^{-i\beta}\sin\vartheta\sinh\gamma \\ ie^{i\beta}\sin\vartheta\sinh\gamma & \cos\vartheta - i\sin\vartheta\cosh\gamma \end{pmatrix}, \tag{71}$$

with $0 \leqslant \vartheta_0, \vartheta, \beta < 2\pi$ and $\gamma \geqslant 0$, or as

$$\hat{U}(T+t_0,t_0) = e^{-i\vartheta_0}\begin{pmatrix} \cosh\vartheta + i\sinh\vartheta\sinh\gamma & -ie^{-i\beta}\sinh\vartheta\cosh\gamma \\ ie^{i\beta}\sinh\vartheta\cosh\gamma & \cosh\vartheta - i\sinh\vartheta\sinh\gamma \end{pmatrix}, \tag{72}$$

with $0 \leqslant \vartheta_0, \beta < 2\pi$ and $\vartheta, \gamma \geqslant 0$. Both these matrices satisfy the condition (67) but their eigenvalues have different character. While in the first case the eigenvalues are given by (70), in the second case one finds that

$$\begin{aligned}\lambda_1 &= e^{-i\vartheta_1} \quad \text{with} \quad \vartheta_1 = \vartheta_0 - i\vartheta,\\ \lambda_2 &= e^{-i\vartheta_2} \quad \text{with} \quad \vartheta_2 = \vartheta_0 + i\vartheta,\end{aligned} \tag{73}$$

where the phases $\vartheta_1, \vartheta_2 \in \mathbb{C}$. In either case we have $\vartheta_1 + \vartheta_2 = 2\vartheta_0$ and $|\lambda_1\lambda_2| = 1$.

In closing, we note that all of the aforementioned parametrized matrices share the same property. Namely, if we denote $\hat{U}(T+t_0,t_0) \equiv \hat{U}(\vartheta_0,\vartheta;\beta,\gamma)$ then it follows from explicit derivations that

$$\begin{aligned}&\hat{U}\big(\vartheta_0^{(1)}+\vartheta_0^{(2)},\vartheta^{(1)}+\vartheta^{(2)};\beta,\gamma\big)\\ &\quad= \hat{U}\big(\vartheta_0^{(1)},\vartheta^{(1)};\beta,\gamma\big)\hat{U}\big(\vartheta_0^{(2)},\vartheta^{(2)};\beta,\gamma\big).\end{aligned} \tag{74}$$

This becomes important in light of Eq. (68). Based on this property, one can show that (for details, see the Appendix and [34])

$$\begin{aligned}\hat{U}(N_{\rm rep}T+t_0,t_0) &= [\hat{U}(\vartheta_0,\vartheta;\beta,\gamma)]^{N_{\rm rep}}\\ &= \hat{U}(N_{\rm rep}\vartheta_0,N_{\rm rep}\vartheta;\beta,\gamma).\end{aligned} \tag{75}$$

This has been already proven in [34] for the fermionic case. We have also realized there that the parameters β and ϑ_0 do not play a role in interpreting the interference patterns in momentum distributions of created pairs. Actually, the parameter ϑ_0 enters the formulas through the global phase factor only. This means that, up to an irrelevant value ϑ_0, the phases of the eigenvalues of the monodromy matrices considered in this paper can be chosen either real [Eq. (70)] or purely complex [Eq. (73)]. We will use this convention when presenting our numerical results. For completeness, let us note that ϑ_0 depends on arbitrarily chosen phases of amplitudes $c_{\boldsymbol{p}}^{(1)}(t)$ and $c_{\boldsymbol{p}}^{(2)}(t)$ in the remote past.

2. *Diffraction and interference terms*

In compliance with our current approach, the momentum distribution of created particles is defined as

$$\mathcal{P}_{N_{\rm rep}}^{(s)} = |\langle -|\hat{U}(+\infty,-\infty)|+\rangle|^2, \tag{76}$$

with the asymptotic in and out states, $|+\rangle = \binom{1}{0}$ and $|-\rangle = \binom{0}{1}$, corresponding to the free particle and antiparticle energy $+\omega_{\boldsymbol{p}}$ and $-\omega_{\boldsymbol{p}}$, respectively. Note that beyond the time interval $(N_{\rm rep}T+t_0,t_0)$ the fields evolve freely. For this reason, Eq. (76) reduces to

$$\mathcal{P}_{N_{\rm rep}}^{(s)} = |\langle -|\hat{U}(N_{\rm rep}T+t_0,t_0)|+\rangle|^2. \tag{77}$$

Using here Eq. (75) with appropriately chosen parametrizations of matrices $\hat{U}$ [Eq. (69), (71), or (72)], we obtain that the momentum distribution of pairs created from vacuum by a sequence of $N_{\rm rep}$ electric-field pulses equals

$$\mathcal{P}_{N_{\rm rep}}^{(s)} = \begin{cases} \sinh^2\gamma\,\sin^2(N_{\rm rep}\vartheta) & \text{for } s=0 \text{ and } \vartheta_1,\vartheta_2\in\mathbb{R}\\ \cosh^2\gamma\,\sinh^2(N_{\rm rep}\vartheta) & \text{for } s=0 \text{ and } \vartheta_1,\vartheta_2\in\mathbb{C},\\ \sin^2\gamma\,\sin^2(N_{\rm rep}\vartheta) & \text{for } s=1/2 \end{cases} \tag{78}$$

while for an individual pulse

$$\mathcal{P}_{1}^{(s)} = \begin{cases} \sinh^2\gamma\,\sin^2\vartheta & \text{for } s=0 \text{ and } \vartheta_1,\vartheta_2\in\mathbb{R}\\ \cosh^2\gamma\,\sinh^2\vartheta & \text{for } s=0 \text{ and } \vartheta_1,\vartheta_2\in\mathbb{C}.\\ \sin^2\gamma\,\sin^2\vartheta & \text{for } s=1/2 \end{cases} \tag{79}$$

Hence, we obtain a standard Fraunhofer-type formula (1), i.e.,

$$\mathcal{P}_{N_{\rm rep}}^{(s)} = \mathcal{P}_{1}^{(s)}\Big[\frac{\sin(N_{\rm rep}\vartheta)}{\sin\vartheta}\Big]^2, \tag{80}$$

which is valid for fermions [34] and for bosons provided that $\vartheta_1, \vartheta_2 \in \mathbb{R}$. Here, we recognize that $\mathcal{P}_1^{(s)}$ plays a role of the diffraction term, while $[\frac{\sin(N_{\rm rep}\vartheta)}{\sin\vartheta}]^2$ is a typical interference term. In contrast, a new type of Fraunhofer formula arises for bosons in the case when $\vartheta_1, \vartheta_2 \in \mathbb{C}$. Namely,

$$\mathcal{P}_{N_{\rm rep}}^{(s)} = \mathcal{P}_{1}^{(s)}\Big[\frac{\sinh(N_{\rm rep}\vartheta)}{\sinh\vartheta}\Big]^2, \tag{81}$$

which also can be obtained from (80) by replacing ϑ by $i\vartheta$. Therefore, by analogy with (80), we shall still interpret $\mathcal{P}_1^{(s)}$ as a diffraction whereas we interpret $[\frac{\sinh(N_{\rm rep}\vartheta)}{\sinh\vartheta}]^2$ as an interference term. Irrespective of the case considered, the latter depends only on the parameter ϑ and the number of pulses in a train. This, in turn, relates to the eigenvalues of the monodromy matrix such that $\vartheta_2 - \vartheta_1 = 2\vartheta$ in Eq. (80) or $\vartheta_2 - \vartheta_1 = 2i\vartheta$ in Eq. (81).

Let us first discuss the case when $\vartheta_2 - \vartheta_1 = 2\vartheta$. It follows from (79) that whenever this phase difference is zero $(\mathrm{mod}\, 2\pi)$, which happens for $\vartheta = n\pi$ where $n = 0, \pm 1, \pm 2, \ldots$, the momentum distribution $\mathcal{P}_1^{(s)}$ vanishes. This is definitely the case for fermions. For bosons, however, it happens provided that $\sinh^2\gamma$ is not simultaneously infinite. The same conclusion can be drawn from Eq. (78) for $\mathcal{P}_{N_{\rm rep}}^{(s)}$, even though in this case additional zeros occur. Now, consider $\bar{\vartheta} = n\pi + \delta\vartheta$ where $\delta\vartheta \ll 1$. This means that there is a small phase difference between both eigenvalues of the monodromy matrix, $\vartheta_2 - \vartheta_1 = 2\delta\vartheta\ (\mathrm{mod} 2\pi)$, known as the *avoided crossing* [34,35]. One can check that for $\bar{\vartheta}$ the interference term in Eq. (80) behaves like

$$\left[\frac{\sin(N_{\rm rep}\vartheta)}{\sin\vartheta}\right]^2\bigg|_{\vartheta=\bar{\vartheta}} \approx N_{\rm rep}^2\left[1 - \frac{1}{3}\left(N_{\rm rep}^2 - 1\right)(\delta\vartheta)^2\right]. \tag{82}$$

Hence, for as long as

$$|\delta\vartheta| \ll \sqrt{\frac{3}{N_{\rm rep}^2 - 1}}, \tag{83}$$

one should observe a nearly perfect coherent enhancement of momentum distributions of produced pairs. Note that perfectly coherent enhancement, i.e., characterized by the scaling factor $N_{\rm rep}^2$, can never be reached. The reason being that, even though the interference term scales like $N_{\rm rep}^2$ when $\vartheta = n\pi$, as shown by our numerical examples, at those points $\mathcal{P}_1^{(s)}$ and $\mathcal{P}_{N_{\rm rep}}^{(s)}$ are both zero. Moreover, it follows from the general theory presented in this section that the momentum distributions calculated for a single pulse (79) should be more regular that the ones induced by a train of pulses (78). This can be inferred from the fact that in between every two subsequent zeros of $\mathcal{P}_1^{(s)}$ there are an additional $(N_{\rm rep} - 1)$ zeros of $\mathcal{P}_{N_{\rm rep}}^{(s)}$. They occur for such parameters for which $\vartheta = n\pi + \frac{m\pi}{N_{\rm rep}}$, where $m = 1, 2, \ldots, (N_{\rm rep} - 1)$. Also, in between two subsequent zeros of $\mathcal{P}_1^{(s)}$ there are $(N_{\rm rep} - 2)$ local maxima of the momentum distributions at $\vartheta = n\pi + \frac{(2m+1)\pi}{2N_{\rm rep}}$, where $m = 1, 2, \ldots, (N_{\rm rep} - 2)$. These are actually minor maxima, observed for $N_{\rm rep} > 2$. Most importantly, the spectra exhibit major maxima for $N_{\rm rep} > 1$, which scale nearly like $N_{\rm rep}^2$ [Eq. (82)]. Note that the aforementioned properties concern the fermionic and bosonic pair production, with some restrictions imposed on the latter. Namely, this is provided that the eigenvalues of the corresponding monodromy matrix (71) have real phases.

Going to the case $\vartheta_2 - \vartheta_1 = 2i\vartheta$, one concludes from Eqs. (78) and (79) that the probability distributions $\mathcal{P}_{N_{\rm rep}}^{(0)}$ and $\mathcal{P}_1^{(0)}$ would be zero at $\vartheta = 0$. As follows from our numerical examples, this is not the case. Surprisingly, when the spectrum of the respective monodromy matrix (72) becomes degenerate $(\vartheta_1 = \vartheta_2)$, the momentum distributions of created bosons do scale as $N_{\rm rep}^2$. We will refer to those points as exceptional points [47,49,50], the reason being that at those points $\cosh^2\gamma$, which enters (78) and (79), tends to infinity; thus, it precludes the distributions from vanishing. While we do not present the respective plot of $\cosh^2\gamma$ in this paper, it has been calculated numerically. Moreover, in the vicinity of exceptional points, i.e., at the avoided crossings $\bar{\vartheta} = \delta\vartheta \ll 1$, the interference term in Eq. (81) becomes

$$\left[\frac{\sinh(N_{\rm rep}\vartheta)}{\sinh\vartheta}\right]^2\bigg|_{\vartheta=\bar{\vartheta}} \approx N_{\rm rep}^2\left[1 + \frac{1}{3}(N_{\rm rep}^2 - 1)(\delta\vartheta)^2\right]. \tag{84}$$

Similarly, for this to occur, Eq. (83) has to hold. In contrast, however, to the previous case, $\mathcal{P}_{N_{\rm rep}}^{(0)}$ exhibits neither additional zeros nor secondary maxima, compared to $\mathcal{P}_1^{(0)}$.

Note that the distributions $\mathcal{P}_{N_{\rm rep}}^{(s)}$ are entirely defined by two angles, γ and ϑ. In order to determine these angles in an experiment, it is enough to know only two distributions, $\mathcal{P}_1^{(s)}$ and $\mathcal{P}_2^{(s)}$, since

$$\begin{aligned}
\sin^2\vartheta &= \frac{4\mathcal{P}_1^{(0)} - \mathcal{P}_2^{(0)}}{4\mathcal{P}_1^{(0)}}, \quad \vartheta_1, \vartheta_2 \in \mathbb{R},\\
\sinh^2\vartheta &= \frac{\mathcal{P}_2^{(0)} - 4\mathcal{P}_1^{(0)}}{4\mathcal{P}_1^{(0)}}, \quad \vartheta_1, \vartheta_2 \in \mathbb{C},\\
\sin^2\vartheta &= \frac{4\mathcal{P}_1^{(1/2)} - \mathcal{P}_2^{(1/2)}}{4\mathrm{P}_1^{(1/2)}}
\end{aligned} \tag{85}$$

and

$$\begin{aligned}
\sinh^2\gamma &= \frac{\mathcal{P}_1^{(0)}}{\sin^2\vartheta}, \quad \vartheta_1, \vartheta_2 \in \mathbb{R},\\
\cosh^2\gamma &= \frac{\mathcal{P}_1^{(0)}}{\sinh^2\vartheta}, \quad \vartheta_1, \vartheta_2 \in \mathbb{C},\\
\sin^2\gamma &= \frac{\mathcal{P}_1^{(1/2)}}{\sin^2\vartheta},
\end{aligned} \tag{86}$$

which follows from our analysis above. These sets of equations define the angles ϑ and γ up to their signs. As we see, for the boson case at the exceptional points, where $4\mathcal{P}_1^{(0)} = \mathcal{P}_2^{(0)}$, we get $\vartheta = 0$ and $\gamma = \pm\infty$. Thus, it fully supports our argument above.

Note that the results presented in this section are not restricted to the process of pair creation. The reason being that our starting point was the set of differential equations (64). We would like to stress that these general equations describe the dynamics (either unitary or pseudounitary) of any two-level system exposed to a time-dependent, repetitive interaction. Therefore, our current predictions do apply to a variety of problems. Having said that, in the next section we will confront these predictions with the numerical results of momenta distributions of pairs extracted from the vacuum by a finite sequence of identical electric-field pulses.

B. Numerical results

In Fig. 3, we present the longitudinal momentum distributions (62) of created particles. In each panel, the upper half represents the spectrum for fermions $\mathcal{P}_{N_{\rm rep}}^{(1/2)}$, whereas the mirror reflected distribution is for bosons $\mathcal{P}_{N_{\rm rep}}^{(0)}$. The spectra in the upper panels have been obtained for a single pulse ($N_{\rm rep} = 1$), whereas the spectra in the lower panels are for a sequence of two such pulses ($N_{\rm rep} = 2$). Here, the Gaussian envelope

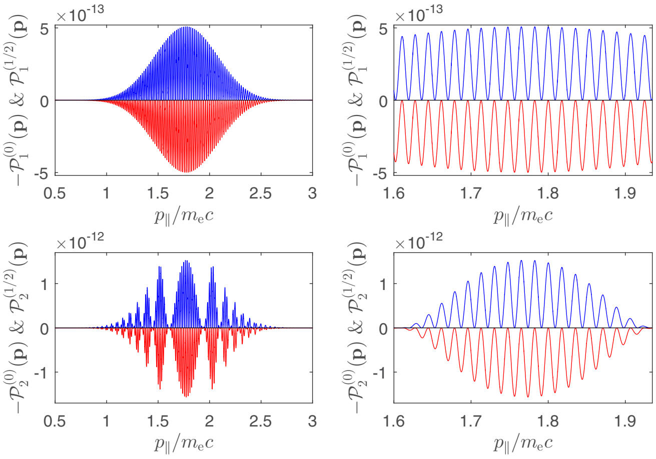

FIG. 3. Longitudinal momentum distributions of fermions $\mathcal{P}^{(1/2)}_{N_{\rm rep}}$ and bosons $\mathcal{P}^{(0)}_{N_{\rm rep}}$ produced by a single ($N_{\rm rep}=1$) and a double ($N_{\rm rep}=2$) Gaussian pulse ($M=1$) with $\sigma=20/t_C$, $T_0=200t_C$, $T=400t_C$, and $\mathcal{E}_0=-0.1\mathcal{E}_S$. In each panel, the upper half shows the spectrum for fermions and the lower half shows the spectrum for bosons. The distributions in the right column are the portions of the distributions from the left column.

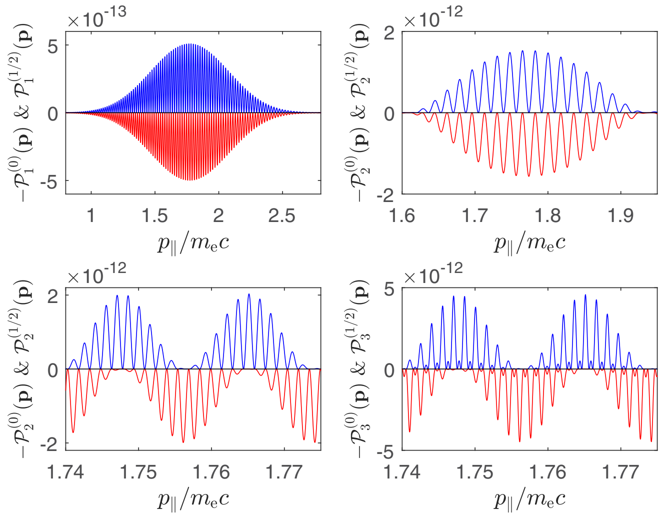

FIG. 4. For comparison, in the upper row we have reproduced the longitudinal momentum distributions of created fermion $\mathcal{P}^{(1/2)}_{N_{\rm rep}}$ and boson pairs $\mathcal{P}^{(0)}_{N_{\rm rep}}$ from Fig. 3. In the left panel, we show the spectra for $N_{\rm rep}=1$, whereas in the right panel we show the spectra for $N_{\rm rep}=2$. We recall that these results are for $T=2T_0$. The spectra for the same field parameters, except that $T=14T_0$, are presented in the lower row. This time, the left panel is for $N_{\rm rep}=2$ and the right panel is for $N_{\rm rep}=3$.

($M=1$) has been used, with the remaining field parameters being $\sigma=20/t_C$, $T_0=200t_C$, $T=400t_C$, and $\mathcal{E}_0=-0.1\mathcal{E}_S$. As shown in Fig. 2, in such case the two half pulses are well separated but, coincidentally, $T=2T_0$. Thus, the spectra of fermions and bosons are shifted by $\pi/2$. Such a shift of the Fraunhofer-like peaks has been seen before and interpreted as originating from different statistics [32]. As we argue below, this is rather accidental and cannot be considered as a statistical effect.

Based on the discussion in Sec. III A, the pattern in the upper row of Fig. 3 will be called the diffraction pattern. This is to emphasize that it originates from interaction of the vacuum with a single electric-field pulse. It is composed of rapid oscillations within a broad envelope. These diffraction peaks are such that the maxima of the distribution for fermions coincide with the zeros of the distribution for bosons; i.e., they are shifted by $\pi/2$. This, however, concerns the diffraction pattern and, as we have checked, is typical for a Gaussian pulse. This is also corroborated by the previous results of Dumlu and Dunne [59,60], who have investigated the pair creation by a single Gaussian pulse with a carrier wave.

If the pairs are created by a train of two pulses, the diffraction pattern is multiplied by the interference term. Thus, within the envelope $\mathcal{P}_1^{(s)}$, we should observe twice that dense series of peaks. Instead, in the lower row of Fig. 3, only an additional modulation of the spectra occurs. We shall show that this is accidental, as the extra interference peaks fall onto the zeros of the diffraction pattern. In addition, irrespective of the statistics, the spectra exhibit a typical $N_{\rm rep}^2$-like scaling predicted by the Fraunhofer formula.

To make our point, in Fig. 4 we confront the spectra presented in Fig. 3 with the spectra calculated for the same field parameters, except that now $T=2800t_C$. In the upper row we show the diffraction peaks (left panel) and the modulated diffraction peaks (right panel) for the case when either a single or a double pulse interacts with the vacuum, and $T=2T_0$. In the lower row, we show that within two diffraction peaks there is a fine peak structure, which originates from the interaction of either two (left panel) or three (right panel) pulses with the vacuum, with $T=14T_0$. Note that for $N_{\rm rep}=2$ this additional structure consists of major maxima, whereas for $N_{\rm rep}=3$ between two such maxima there appears a minor one. This is a typical interference pattern predicted by the Fraunhofer formula (80). Most importantly, while the diffraction peaks are shifted by $\pi/2$, the interference peaks for fermions and bosons coincide. This clearly indicates that the respective shift of the bosonic and fermionic distributions is closely related to the parameters of the driving laser field, rather than to the statistics of created particles. We have confirmed this for other parameters as well. For instance, in Fig. 5 we present the longitudinal momentum distributions for a Gaussian (upper row) and a super-Gaussian envelope ($M=5$, lower row) for $\sigma=5/t_C$, $T_0=40t_C$, $T=357t_C$, and $\mathcal{E}_0=-0.1\mathcal{E}_S$. One can see that sometimes the bosonic and fermionic spectra match very closely. This is the case of particles created from the vacuum by a sequence of two pulses (right column). For a single Gaussian pulse, there is a $\pi/2$ shift between both momentum distributions. However, for a super-Gaussian pulse, there is a momentum region where both spectra coincide, but then they exhibit a shift which varies with the particle momentum. Interestingly, the results for a super-Gaussian envelope are by five orders of magnitude larger than for a Gaussian envelope (similar enhancement has been discussed in [61]). Since the shape effects are not the topic of this paper, they will be analyzed elsewhere. Here, we shall look more closely into the peak structure of the presented momentum distributions.

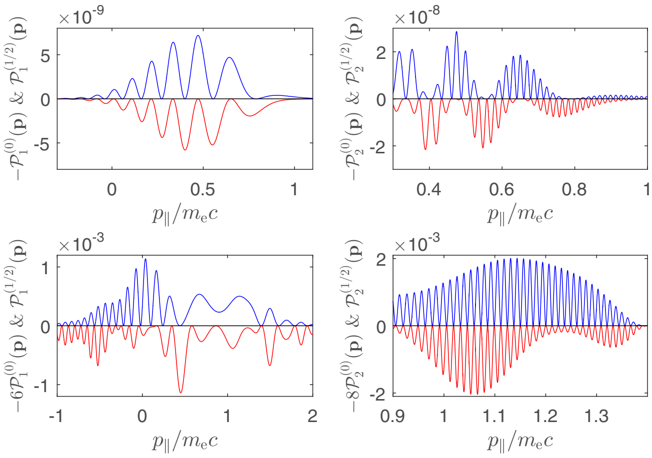

FIG. 5. Longitudinal momentum spectra of fermions $\mathcal{P}^{(1/2)}_{N_{\rm rep}}$ (upper half in each panel) and bosons $\mathcal{P}^{(0)}_{N_{\rm rep}}$ (lower half in each panel) for the external field parameters: $\sigma = 5/t_C$, $T_0 = 40t_C$, $T = 357t_C$, and $\mathcal{E}_0 = -0.1\mathcal{E}_S$. The results for Gaussian ($M = 1$) and super-Gaussian ($M = 5$) shaped pulses are shown in the upper and the lower rows, respectively. For $M = 1$ we observe that the diffraction maxima are shifted by $\pi/2$, whereas the interference maxima coincide with each other. Such a general rule cannot be formulated for $M = 5$. For instance, for the diffraction pattern (bottom left panel) there are momentum regions ($p_\parallel < 0.3m_ec$ and $p_\parallel > 1.2m_ec$) where the peaks in the fermionic and bosonic spectra coincide, the region ($0 < p_\parallel < 0.3m_ec$) where they are shifted by roughly $\pi/2$, and the region $0.3m_ec < p_\parallel < 1.2m_ec$ where both spectra exhibit slow modulations. On the other hand, both distributions $\mathcal{P}^{(s)}_2$ (bottom right panel) peak at the same values of $p_\parallel$.

C. Interpretation of the results

We have demonstrated numerically that the $N^2_{\rm rep}$-type enhancement of the momentum spectra of created particles is observed independently of their statistics. This is supported by Eqs. (80) and (81) and the analysis of phases ϑ_1 and ϑ_2 around the avoided crossings (see Sec. III A). In Fig. 6, in both panels we present these phases as functions of the longitudinal momentum of created bosons (dashed red curve) and fermions (solid blue curve). The upper panel is for the Gaussian ($M = 1$) whereas the lower panel is for the super-Gaussian ($M = 5$) envelope. The remaining parameters are the same as in Fig. 5, and $N_{\rm rep} = 1$. Note that, on the scale of the figures, the solid and dashed curves are essentially the same. In other words, there is no obvious difference between the eigenvalues determining the time evolution of the bosonic and fermionic fields. This is quite surprising taking into account that there is a fundamental difference between both theories. Namely, while the time evolution for the fermionic field is unitary, for the bosonic field it is pseudounitary (for more details, see the Appendix and [34]). Since the difference between the respective phases is nearly zero, the crossings and the avoided crossings in both cases occur at roughly the same values of $p_\parallel$. This should result in a very similar interference pattern, which is confirmed in the right column of Fig. 5. In this column the so-called interference maxima and the zeros of the distributions are basically the same, even though the diffraction patterns with their own peaks and zeros might differ.

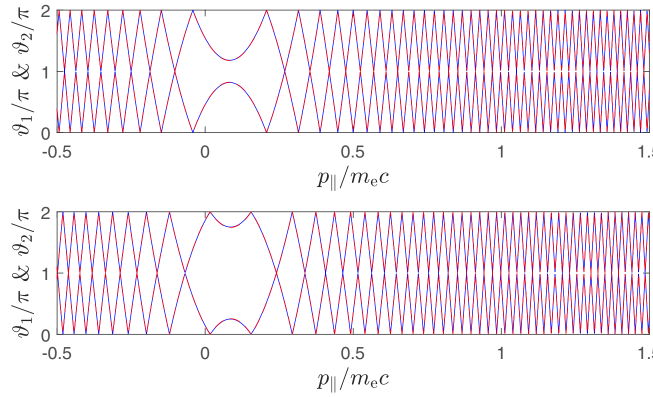

FIG. 6. The phases of eigenvalues of the monodromy matrix for $\sigma = 5/t_C, T_0 = 40t_C, T = 357t_C, \mathcal{E}_0 = -0.1\mathcal{E}_S, N_{\rm rep} = 1$, and $M = 1$ (upper panel) or $M = 5$ (lower panel). In each panel there are two lines: a solid blue line for spinor QED and the dashed red line for scalar QED. On the scale of the figure these lines are identical, which occurs also for other parameters of the external field. In both cases and nearly for the same values of $p_\parallel$ we observe either true avoided crossings (for fermions) or pseudoavoided crossings (for bosons). As it follows from the general theory formulated in Sec. III A, both types of avoided crossings lead to coherentlike enhancements in the momentum distribution of created pairs.

An analysis of phases ϑ_1 and ϑ_2 for the case considered in Fig. 3 predicts the same: The interference pattern should look similar irrespective of the statistics. At first glance, this is not the case in Fig. 3. We have confronted this figure with the positions of avoided crossings. It turns out that every avoided crossing coincides interchangeably with the zero or the maximum of the diffraction pattern. For this reason, the spectra in Fig. 3 are missing every other interference peak, which invalidates the conclusion of [32]. As it follows from our analysis, the positions of interference peaks are nearly the same for bosons and fermions. They are modulated, however, by the diffraction term that depends on the particle statistics and on the parameters of the external field.

We have demonstrated that the positions of avoided crossings of the phases ϑ_1 and ϑ_2 are basically the same. In order to see a more pronounced difference between both types of avoided crossings, in Fig. 7 we plot them for a stronger electric field and for a super-Gaussian pulse. More specifically, these results have been obtained for $\sigma = 10/t_C$, $T_0 = 10t_C$, $T = 200t_C$, $\mathcal{E}_0 = -0.5\mathcal{E}_S$, and $M = 5$. In this figure, the dependence of the phases on the longitudinal momentum of created particles around a chosen avoided crossing is presented for either fermions (top left panel) or bosons (remaining panels). As denoted in each panel, the results illustrate the behavior of ϑ_1 and ϑ_2 for the cases when the pair creation is stimulated by either a single ($N_{\rm rep} = 1$), a double ($N_{\rm rep} = 2$), or a triple ($N_{\rm rep} = 3$) electric-field pulse. Note that here $\vartheta_0 = \pi$, and so the total global phase accumulated over the entire field duration is $N_{\rm rep}\pi$. For this reason, on the vertical axis we subtract $N_{\rm rep}$ from $\vartheta_{1,2}/\pi$. In the fermionic case, we observe an actual avoided crossing, with a small gap that increases linearly with the number of pulses in the pulse sequence (see also [34]). The phases in the bosonic case reveal a different behavior around what we call a *pseudoavoided*

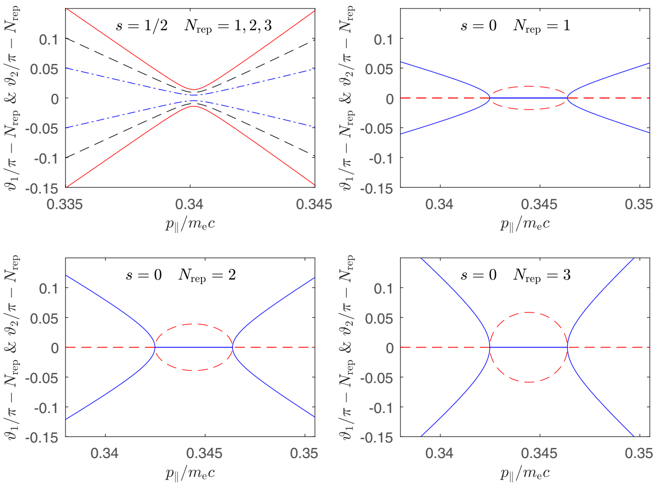

FIG. 7. The phases of the eigenvalues of monodromy matrices for fermions (top left panel) and bosons (remaining panels) in the case when the pairs are created by a train of $N_{\rm rep}$ electric super-Gaussian pulses ($M = 5$) such that $\sigma = 10/t_C$, $T_0 = 10t_C$, $T = 200t_C$, and $\mathcal{E}_0 = -0.5\mathcal{E}_S$. We show a true avoided crossing for fermions, with a nonzero gap between the phases which grows linearly with $N_{\rm rep}$ (here, the dash-dotted line is for $N_{\rm rep} = 1$, the dashed line is for $N_{\rm rep} = 2$, whereas the solid line is for $N_{\rm rep} = 3$). Pseudoavoided crossings for bosons have very distinct features, as they occur in the vicinity of exceptional points at which the phases ϑ_j ($j = 1, 2$) turn from being real to being purely imaginary. Here, the real and imaginary parts of the phases are plotted as solid and dashed lines, respectively. Note that the phase difference in the complex regime also grows linearly with $N_{\rm rep}$.

crossing. Around such crossing, the phases ϑ_1 and ϑ_2 change from real (solid line) to complex (dashed line) values. This happens at the exceptional points. In between them, there is a single pseudoavoided crossing where we observe a nearly perfect coherent enhancement in agreement with Eq. (81). Note also that, similar to the fermionic case, the corresponding gap increases linearly with $N_{\rm rep}$. In both cases it holds also that $\vartheta_1 + \vartheta_2 = 0 \bmod 2\pi$. Finally, we note that a peculiar behavior of phases in the bosonic case is observed in a very narrow momentum interval. Except for such intervals, the phases take real values and their behavior is determined by (80). Thus, while the major interference peaks can be attributed to pseudoavoided crossings, the other features of the interference pattern are the same as in the fermionic case. The same stays true for other field parameters as well, provided that the electric pulses are well separated, i.e., $T \gg T_0$.

To demonstrate a very good agreement of our numerical results with the general theory presented in Sec. III A, we plot the momentum distributions around the avoided crossings analyzed in Fig. 7. In Fig. 8, we show the corresponding distributions for fermions (left panel) and bosons (right panel) when the pairs are generated by various pulse configurations: $N_{\rm rep} = 1$ (dash-dotted line), $N_{\rm rep} = 2$ (dashed line), and $N_{\rm rep} = 3$ (solid line). In the regions of $p_\parallel$ where the phases ϑ_j ($j = 1, 2$) are real, the curves decrease in magnitude with increasing $N_{\rm rep}$. This is in agreement with the approximation originated from the standard Fraunhofer formula (82), as the gap between both phases increases linearly with $N_{\rm rep}$ (with

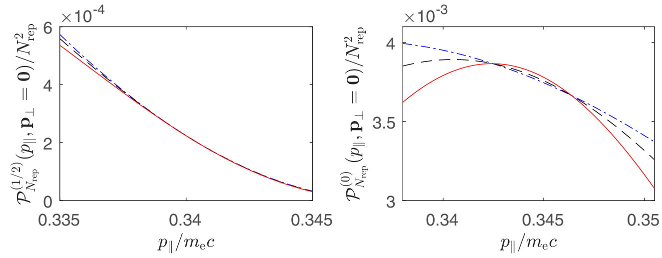

FIG. 8. The momentum distributions of created fermions (left panel) and bosons (right panel) near the avoided crossings shown in Fig. 7. The distributions are scaled by $N_{\rm rep}^2$. The dash-dotted line is for $N_{\rm rep} = 1$, the dashed line is for $N_{\rm rep} = 2$, whereas the solid line corresponds to $N_{\rm rep} = 3$. For fermions, the phase difference is small enough so the approximation (82) is well satisfied. For bosons, there are two momenta $p_\parallel$ for which all the distributions take the same value. Rather than that, they follow either the approximation (82) or (84) depending on the momentum interval. As explained in the text, at these two values of $p_\parallel$ the bosonic spectra are coherently enhanced. This is different than in the fermionic case, when the strictly coherent enhancement can never be observed.

a small negative, cubic correction). On the other hand, in the momentum interval where the phases ϑ_j are complex, which is in a very small momentum interval for bosons, we observe the opposite tendency. Here, the curves increase in magnitude with increasing $N_{\rm rep}$, as the phase difference $(\vartheta_2 - \vartheta_1)$ in Eq. (84) increases linearly with $N_{\rm rep}$ (with a small positive, qubic correction). Interestingly, for bosons there are two values of longitudinal momentum where all momentum distributions, when scaled by $N_{\rm rep}^2$, take the same value. This happens at exactly the same momenta for which $\vartheta_1 = \vartheta_2$ in Fig. 7, i.e., at the exceptional points. According to the general theorem introduced in Sec. III A, when the phase difference is strictly zero ($\vartheta = 0$) the respective momentum distributions should be zero as well. We observe, however, that at both crossings the spectra take nonzero values. The reason being that at these two points the parameter γ in (78) and (79) becomes infinitely large. As a consequence, a fully coherent enhancement of the bosonic spectra is observed at the exceptional points. This feature distinguishes the bosonic and fermionic momentum distributions and, as such, can surely be regarded as a statistical effect. It also means that for fermions the nearly perfect coherent enhancement can be lost by changing the parameters of the electric field, such as the number of pulses in a train. For bosons, however, this is not the case.

IV. CONCLUSIONS

We have studied the creation of bosonic and fermionic pairs by a finite sequence of $N_{\rm rep}$ identical, time-dependent electric-field pulses. In the case considered in this paper, i.e., when the pulses are linearly polarized, both problems simplify to solving a two-level system of equations for time evolution of a single field eigenmode. The difference is that the time-evolution matrix is either unitary for fermions or pseudounitary for bosons. This also affects the resulting momentum distributions of particles, which has been studied in this paper in great detail.

In relation to our problem, we have formulated a general theory of a two-level system exposed to a periodic, but finite, time-dependent interaction. The distinction between unitary and pseudounitary time evolution was made. In both cases, we have derived the Fraunhofer-type formulas describing the interlevel transitions. These formulas have been used then to interpret our numerical results of momentum distributions of created pairs.

In analogy to the standard Fraunhofer formula (1), the momentum distributions of produced particles exhibit the interference peaks which are modulated by the diffraction pattern. Whereas the major interference peaks in the fermionic case do not follow strictly an $N_{\rm rep}^2$ scaling, it does happen for bosons. In both cases, this has been attributed to adiabatic transitions at avoided crossings of the phases defining the time-evolution matrix. The difference is the avoided crossing itself. For bosons, for instance, it is observed at the passage between real and imaginary phases. When this happens, the perfect $N_{\rm rep}^2$ enhancement of momentum distributions of created bosons is observed.

When analyzing the momentum distributions of created particles we have observed that, for the Gaussian pulse profile, the diffraction patterns for bosons and fermions are shifted such that maxima of the former correspond to zeros of the latter. This seems quite coincidental, as already for the super-Gaussian pulse profile it is not true. Regardless, the diffraction pattern does modulate the interference peaks and so it influences the overall structure of momentum distributions. Still the interference pattern looks nearly identical for fermions and bosons.

ACKNOWLEDGMENT

This work is supported by the National Science Centre (Poland) under Grant No. 2014/15/B/ST2/02203.

APPENDIX: SU(1, 1) GROUP

Elements of the SU(1, 1) group are 2×2 complex matrices, $\hat{U}$, which satisfy the following relation:

$$\hat{U}^{\ddagger} = \hat{U}^{-1}, \tag{A1}$$

where the pseudo-Hermitian conjugate of $\hat{U}$ has been defined in (66). One can also prove that the eigenvalues λ_j ($j = 1, 2$) of the matrix $\hat{U}$ are such that $|\lambda_1\lambda_2| = 1$.

Applying the above definition to the general matrix,

$$\hat{U} = \begin{pmatrix} U_{11} & U_{12} \\ U_{21} & U_{22} \end{pmatrix}, \tag{A2}$$

we conclude that the matrix elements $U_{j\ell}$ ($j, \ell = 1, 2$) have to fulfill the conditions

$$\begin{aligned} |U_{11}|^2 - |U_{21}|^2 &= 1, \\ |U_{22}|^2 - |U_{12}|^2 &= 1, \\ U_{11}^* U_{12} - U_{21}^* U_{22} &= 0. \end{aligned} \tag{A3}$$

This actually means that the matrix $\hat{U}$ can be uniquely defined by four real parameters. It turns out that one can introduce these parameters such that

$$\hat{U} = e^{-i\vartheta_0}\begin{pmatrix} \cos\vartheta + i\sin\vartheta\cosh\gamma & -ie^{-i\beta}\sin\vartheta\sinh\gamma \\ ie^{i\beta}\sin\vartheta\sinh\gamma & \cos\vartheta - i\sin\vartheta\cosh\gamma \end{pmatrix}, \tag{A4}$$

where $0 \leqslant \vartheta_0, \vartheta, \beta < 2\pi$ and $\gamma \geqslant 0$. Another possibility is

$$\hat{U} = e^{-i\vartheta_0}\begin{pmatrix} \cosh\vartheta + i\sinh\vartheta\sinh\gamma & -ie^{-i\beta}\sinh\vartheta\cosh\gamma \\ ie^{i\beta}\sinh\vartheta\cosh\gamma & \cosh\vartheta - i\sinh\vartheta\sinh\gamma \end{pmatrix}, \tag{A5}$$

with $0 \leqslant \vartheta_0, \beta < 2\pi$ and $\vartheta, \gamma \geqslant 0$. Transition between these two representations occurs through the exceptional point, at which $\vartheta = 0$ and $\gamma = \infty$, with the substitutions $\vartheta \to i\vartheta$, $\cosh\gamma \to -i\sinh\gamma$, and $\sinh\gamma \to -i\cosh\gamma$. Below, we discuss consequences of each parametrization.

1. Real phases of the eigenvalues

For the matrix (A4), there are two complex eigenvalues, $\lambda_1 = e^{-i(\vartheta_0-\vartheta)}$ and $\lambda_2 = e^{-i(\vartheta_0+\vartheta)}$, with real phases $(\vartheta_0 \mp \vartheta)$. The corresponding eigenvectors are

$$\begin{aligned} |1\rangle &= e^{i\psi_1}\begin{pmatrix} e^{-i\beta/2}\cosh(\gamma/2) \\ e^{i\beta/2}\sinh(\gamma/2) \end{pmatrix}, \\ |2\rangle &= e^{i\psi_2}\begin{pmatrix} e^{-i\beta/2}\sinh(\gamma/2) \\ e^{i\beta/2}\cosh(\gamma/2) \end{pmatrix}, \end{aligned} \tag{A6}$$

which are defined up to irrelevant phase factors, $0 \leqslant \psi_1, \psi_2 < 2\pi$. In other words, it holds that $\hat{U}|j\rangle = \lambda_j|j\rangle$, where $j = 1, 2$ and $|\lambda_j| = 1$ in agreement with the general statement that $|\lambda_1\lambda_2| = 1$. The eigenstates (A6) are linearly independent and orthonormal in the sense that

$$\langle\langle\chi_1|\chi_2\rangle\rangle = \langle\chi_1|\hat{\sigma}_3|\chi_2\rangle \tag{A7}$$

defines the pseudoscalar product for arbitrary complex column vectors, $|\chi_j\rangle$, $j = 1, 2$. Using this definition, one derives that

$$\langle\langle 1|1\rangle\rangle = 1, \quad \langle\langle 2|2\rangle\rangle = -1, \quad \langle\langle 1|2\rangle\rangle = 0 = \langle\langle 2|1\rangle\rangle. \tag{A8}$$

In compliance with Eq. (A7), we construct the pseudoprojectors onto the given eigenstate $|j\rangle$ such that

$$\hat{P}_1 = |1\rangle\langle 1|\hat{\sigma}_3, \quad \hat{P}_2 = -|2\rangle\langle 2|\hat{\sigma}_3. \tag{A9}$$

In our case, this gives

$$\begin{aligned} \hat{P}_1 &= \frac{1}{2}\begin{pmatrix} 1+\cosh\gamma & -e^{-i\beta}\sinh\gamma \\ e^{i\beta}\sinh\gamma & 1-\cosh\gamma \end{pmatrix}, \\ \hat{P}_2 &= \frac{1}{2}\begin{pmatrix} 1-\cosh\gamma & e^{-i\beta}\sinh\gamma \\ -e^{i\beta}\sinh\gamma & 1+\cosh\gamma \end{pmatrix}. \end{aligned} \tag{A10}$$

With these definitions, we obtain

$$\hat{P}_j^{\ddagger} = \hat{P}_j, \quad \hat{P}_j\hat{P}_\ell = \hat{P}_j\delta_{j\ell}, \quad \hat{P}_1 + \hat{P}_2 = \hat{I}. \tag{A11}$$

In addition, the spectral decomposition holds:

$$\hat{U} = \lambda_1\hat{P}_1 + \lambda_2\hat{P}_2. \tag{A12}$$

At this point, it is important to stress that for $\vartheta = 0$ the spectrum of $\hat{U}$ is degenerate; namely, $\lambda_1 = \lambda_2$. It follows from the above definitions that in this case the matrix $\hat{U}$ becomes trivial, $\hat{U} = \lambda_1\hat{I}$. We also note that, due to the properties of the pseudoprojection operators (A11), the matrix $\hat{U}$ raised to the power N is

$$\hat{U}^N = \lambda_1^N\hat{P}_1 + \lambda_2^N\hat{P}_2, \tag{A13}$$

or, more generally, for any analytic function f we have

$$f(\hat{U}) = f(\lambda_1)\hat{P}_1 + f(\lambda_2)\hat{P}_2. \tag{A14}$$

Equation (A13) will be of particular importance in Sec. III.

2. Complex phases of the eigenvalues

For the matrix (A5), the corresponding eigenvalues are $\lambda_1 = e^{-i(\vartheta_0+i\vartheta)}$ and $\lambda_2 = e^{-i(\vartheta_0-i\vartheta)}$, meaning that their phases $(\vartheta_0 \mp i\vartheta)$ are complex. The peculiar feature of the matrix (A5) is that the corresponding eigenvectors cannot be normalized in the sense of Eq. (A7). Namely, their norm is zero. Nevertheless, one can introduce another system of the pseudoprojection operators:

$$\hat{P}_1 = \frac{1}{2}\begin{pmatrix} 1 + i\sinh\gamma & -ie^{-i\beta}\cosh\gamma \\ ie^{i\beta}\cosh\gamma & 1 - i\sinh\gamma \end{pmatrix},$$
$$\hat{P}_2 = \frac{1}{2}\begin{pmatrix} 1 - i\sinh\gamma & ie^{-i\beta}\cosh\gamma \\ -ie^{i\beta}\cosh\gamma & 1 + i\sinh\gamma \end{pmatrix}, \tag{A15}$$

such that

$$\hat{P}_1^{\ddagger} = \hat{P}_2, \quad \hat{P}_2^{\ddagger} = \hat{P}_1, \quad \hat{P}_j\hat{P}_\ell = \hat{P}_j\delta_{j\ell}, \quad \hat{P}_1 + \hat{P}_2 = \hat{I}. \tag{A16}$$

This means that the spectral decomposition (A12) and its consequences still hold. In closing we note that, similarly to the case considered in Appendix A1, for $\vartheta = 0$ the eigenvalues of the matrix (A5) are degenerate $\lambda_1 = \lambda_2 = e^{-i\vartheta_0}$ and the matrix (A5) becomes trivial.

[1] F. S. Crawford, *Waves* (McGraw-Hill, New York, 1968).
[2] J. W. S. Rayleigh, *The Theory of Sound* (MacMillan, London, 1894), Vol. 1.
[3] G. B. Whitham, *Linear and Nonlinear Waves* (Wiley, New York, 1974).
[4] M. Born and E. Wolf, *Principles of Optics* (Pergamon, Oxford, 1968).
[5] F. Frémont, *Young-Type Interferences with Electrons* (Springer-Verlag, Berlin, 2014).
[6] M. A. Van Hove, W. H. Weinberg, and C. M. Chan, *Low-Energy Electron Diffraction* (Springer-Verlag, Berlin, 1986).
[7] M. P. Silverman, *More Than One Mystery: Explorations in Quantum Interference* (Springer-Verlag, New York, 1995).
[8] M. P. Silverman, *Quantum Superposition* (Springer, Berlin, 2008).
[9] P. Deymier and K. Runge, *Sound Topology, Duality, Coherence and Wave-Mixing* (Springer, Cham, 2017).
[10] R. Peierls, *Surprises in Theoretical Physics* (Princeton University, Princeton, NJ, 1979).
[11] V. Barone and E. Predazzi, *High-Energy Particle Diffraction* (Springer-Verlag, Berlin, 2002).
[12] A. P. Potylitsyn, M. I. Ryazanov, M. N. Strikhanov, and A. A. Tishchenko, *Diffraction Radiation from Relativistic Particles* (Springer-Verlag, Berlin, 2010).
[13] S. J. Smith and E. M. Purcell, Phys. Rev. **92**, 1069 (1953).
[14] G. P. Williams, Rep. Prog. Phys. **69**, 301 (2006).
[15] K. Krajewska, M. Twardy, and J. Z. Kamiński, Phys. Rev. A **89**, 052123 (2014).
[16] F. Cajiao Vélez, J. Z. Kamiński, and K. Krajewska, Atoms **7**, 34 (2019).
[17] K. Krajewska, F. Cajiao Vélez, and J. Z. Kamiński, Phys. Rev. A **91**, 062106 (2015).
[18] K. Krajewska and J. Z. Kamiński, Phys. Rev. A **90**, 052108 (2014).
[19] F. Cajiao Vélez, K. Krajewska, and J. Z. Kamiński, Phys. Rev. A **91**, 053417 (2015).
[20] K. Krajewska and J. Z. Kamiński, Phys. Lett. A **380**, 1247 (2016).
[21] F. Sauter, Z. Phys. **69**, 742 (1931).
[22] W. Heisenberg and H. Euler, Z. Phys. **98**, 714 (1936).
[23] J. S. Schwinger, Phys. Rev. **82**, 664 (1951).
[24] W. Greiner, B. Müller, and J. Rafelski, *Quantum Electrodynamics of Strong Fields* (Springer-Verlag, Berlin, 1985).
[25] J. Rafelski, L. P. Fulcher, and A. Klein, Phys. Rep. **38**, 227 (1978).
[26] P. Koch, B. Müller, and J. Rafelski, Phys. Rep. **142**, 167 (1986).
[27] J. Rafelski, *Relativity Matters* (Springer, Cham, 2017).
[28] *Dirac Matter*, edited by B. Duplantier, V. Rivasseau, and J.-N. Fuchs (Birkhäuser, Cham, 2017).
[29] A. H. Castro Neto, F. Guinea, N. M. R. Peres, K. S. Novoselov, and A. K. Geim, Rev. Mod. Phys. **81**, 109 (2009).
[30] F. Hebenstreit, R. Alkofer, G. V. Dunne, and H. Gies, Phys. Rev. Lett. **102**, 150404 (2009).
[31] E. Akkermans and G. V. Dunne, Phys. Rev. Lett. **108**, 030401 (2012).
[32] Z. L. Li, D. Lu, and B. S. Xie, Phys. Rev. D **89**, 067701 (2014).
[33] Z. L. Li, D. Lu, B. S. Xie, L. B. Fu, J. Liu, and B. F. Shen, Phys. Rev. D **89**, 093011 (2014).
[34] J. Z. Kamiński, M. Twardy, and K. Krajewska, Phys. Rev. D **98**, 056009 (2018).
[35] K. Krajewska, W. Gac, M. Twardy, and J. Z. Kamiński, J. Phys.: Conf. Series **1206**, 012018 (2019).
[36] A. Ilderton, arXiv:1910.03012.
[37] S. Schmidt, D. Blaschke, G. Röpke, S. A. Smolyansky, A. V. Prozorkevich, and V. D. Toneev, Int. J. Mod. Phys. E **7**, 709 (1998).
[38] K. Wódkiewicz and J. H. Eberly, J. Opt. Soc. Am. B **2**, 458 (1985).

[39] K. G. Makris, R. El-Ganainy, D. N. Christodoulides, and Z. H. Musslimani, Phys. Rev. Lett. **100**, 103904 (2008).
[40] A. Guo, G. J. Salamo, D. Duchesne, R. Morandotti, M. Volatier-Ravat, V. Aimez, G. A. Siviloglou, and D. N. Christodoulides, Phys. Rev. Lett. **103**, 093902 (2009).
[41] C. E. Rüter, K. G. Makris, R. El-Ganainy, D. N. Christodoulides, M. Segev, and D. Kip, Nat. Phys. **6**, 192 (2010).
[42] Y.-C. Lee, J. Liu, Y.-L. Chuang, M.-H. Hsieh, and R.-K. Lee, Phys. Rev. A **92**, 053815 (2015).
[43] B. Peng, S. K. Ozdemir, S. Rotter, H. Yilmaz, M. Liertzer, F. Monifi, C. M. Bender, F. Nori, and L. Yang, Science **346**, 328 (2014).
[44] L. Feng, Z. J. Wong, R.-M. Ma, Y. Wang, and X. Zhang, Science **346**, 972 (2014).
[45] B. T. Torosov and N. V. Vitanov, Phys. Rev. A **96**, 013845 (2017).
[46] R. Grimaudo, A. S. M. de Castro, M. Kuś, and A. Messina, Phys. Rev. A **98**, 033835 (2018).
[47] I. Rotter, J. Phys. A **42**, 153001 (2009).
[48] N. Moiseyev, *Non-Hermitian Quantum Mechanics* (Cambridge University, Cambridge, England, 2011).
[49] I. Rotter and J. P. Bird, Rep. Prog. Phys. **78**, 114001 (2015).
[50] L. Praxmeyer, P. Yang, and R.-K. Lee, Phys. Rev. A **93**, 042122 (2016).
[51] A. A. Grib, S. G. Mamaev, and V. M. Mostepanenko, *Vacuum Quantum Effects in Strong External Fields* (Atomizdat, Moscow, 1988).
[52] A. A. Grib, V. M. Mostepanenko, and V. M. Frolov, Teor. Mat. Fiz. **13**, 1207 (1972).
[53] W. Greiner, *Relativistic Quantum Mechanics* (Springer-Verlag, Berlin, 2000).
[54] W. Greiner and J. Reinhardt, *Quantum Electrodynamics* (Springer-Verlag, Berlin, 2009).
[55] C. J. Pethick and H. Smith, *Bose-Einstein Condensation in Dilute Gases* (Cambridge University, Cambridge, England, 2002).
[56] I. Bialynicki-Birula, P. Górnicki, and J. Rafelski, Phys. Rev. D **44**, 1825 (1991).
[57] I. Białynicki-Birula and L. Rudnicki, Phys. Rev. D **83**, 065020 (2011).
[58] V. A. Yakubovich and V. M. Starzhinskii, *Linear Differential Equations with Periodic Coefficients* (Wiley, New York, 1975).
[59] C. K. Dumlu and G. V. Dunne, Phys. Rev. Lett. **104**, 250402 (2010).
[60] C. K. Dumlu and G. V. Dunne, Phys. Rev. D **83**, 065028 (2011).
[61] I. Akal, arXiv:1712.05368v2.